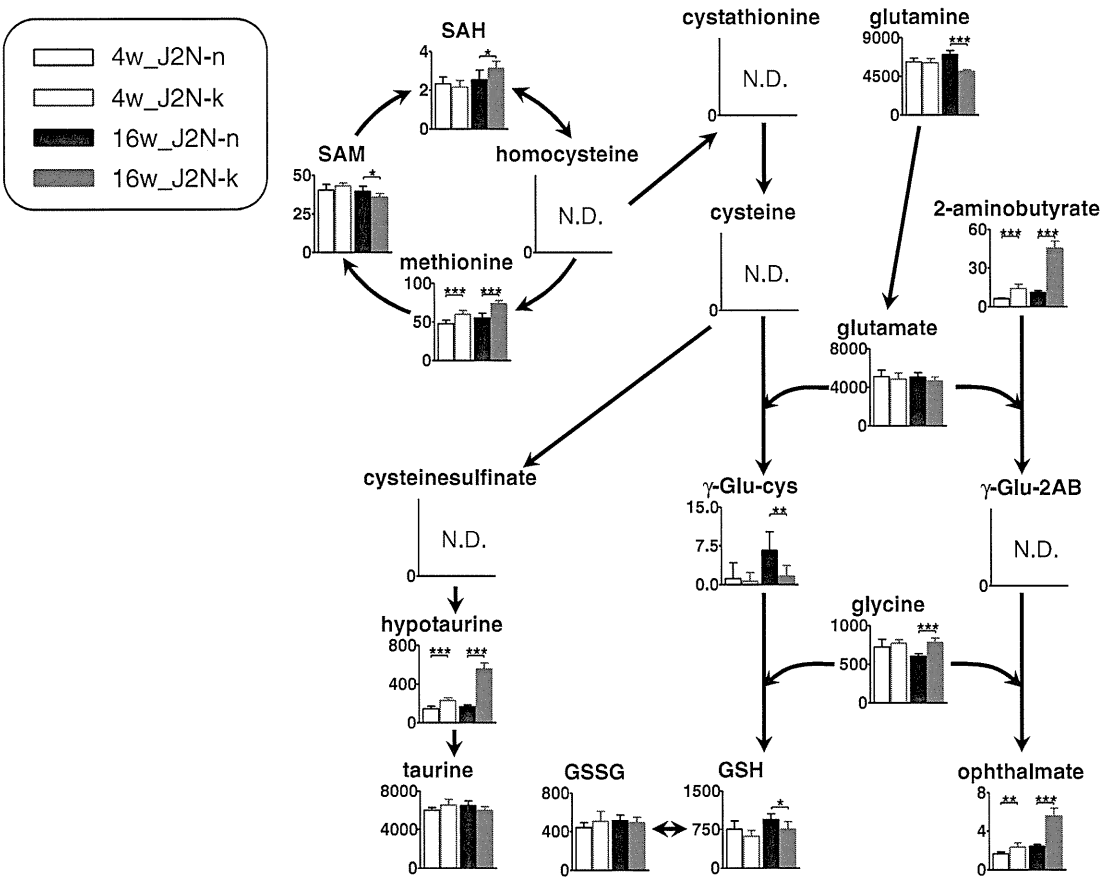

Fig. 3. Quantification of metabolites involved in GSH biosynthesis and related pathways. The columns represent average concentrations (nmol/g tissue), and the error bars indicate SD. *$p<0.05$; **$p<0.01$; ***$p<0.001$; and N.D., not detected.

such as 18:1/18:2PE (0.7-fold, $p=1.5\times10^{-3}$), and 18:0p/20:5PE (0.4-fold, $p=1.0\times10^{-5}$), were markedly reduced in J2N-k tissues at 16 weeks. Thus, the levels of PC and PE species commonly containing linoleic acid (18:2) or EPA (20:5) were reduced at the onset of DCM.

Marked differences between the SM levels and their Cer metabolites were observed in the 2 hamster strains at 16 weeks. For example, the levels of 34:1SM (d18:1/16:0; 1.4-fold, $p=5.1\times10^{-4}$) and 34:1Cer (1.4-fold, $p=4.9\times10^{-2}$) increased, but those of 38:1SM (d18:1/20:0; 0.7-fold, $p=3.3\times10^{-3}$) and 38:1Cer (0.6-fold, $p=3.1\times10^{-3}$) decreased in J2N-k tissue as compared to J2N-n tissue.

The levels of major TAG species significantly decreased in J2N-k compared with J2N-n tissues at 16 weeks (Fig. 5, Supplementary Table 3). Although we could not determine the individual fatty acid chain compositions, many of these species were dramatically decreased, including 54:5TAG (0.5-fold, $p=6.0\times10^{-3}$) and 54:6TAG (0.5-fold, $p=5.4\times10^{-3}$). Furthermore, the levels of 9 DAG species

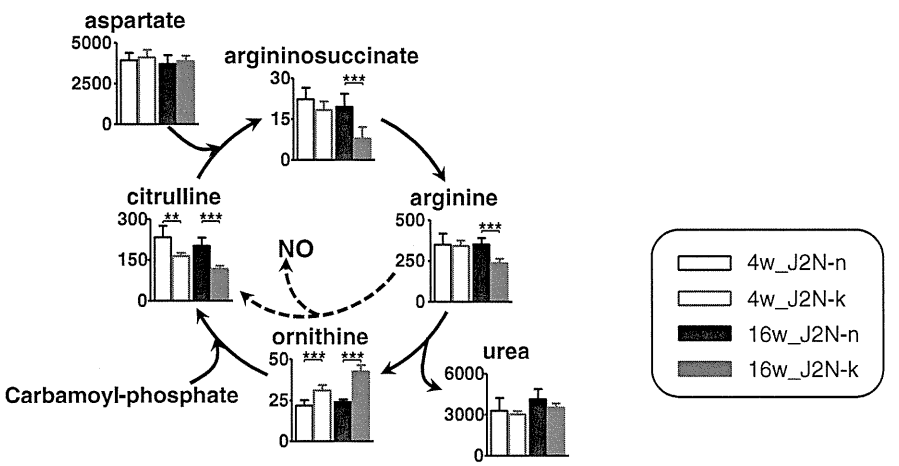

Fig. 4. Metabolic changes in urea cycle metabolism. The dashed lines indicate the NO synthesis pathway, columns represent average concentrations (nmol/g tissue), and error bars indicate SD. *$p<0.05$; **$p<0.01$; and ***$p<0.001$.

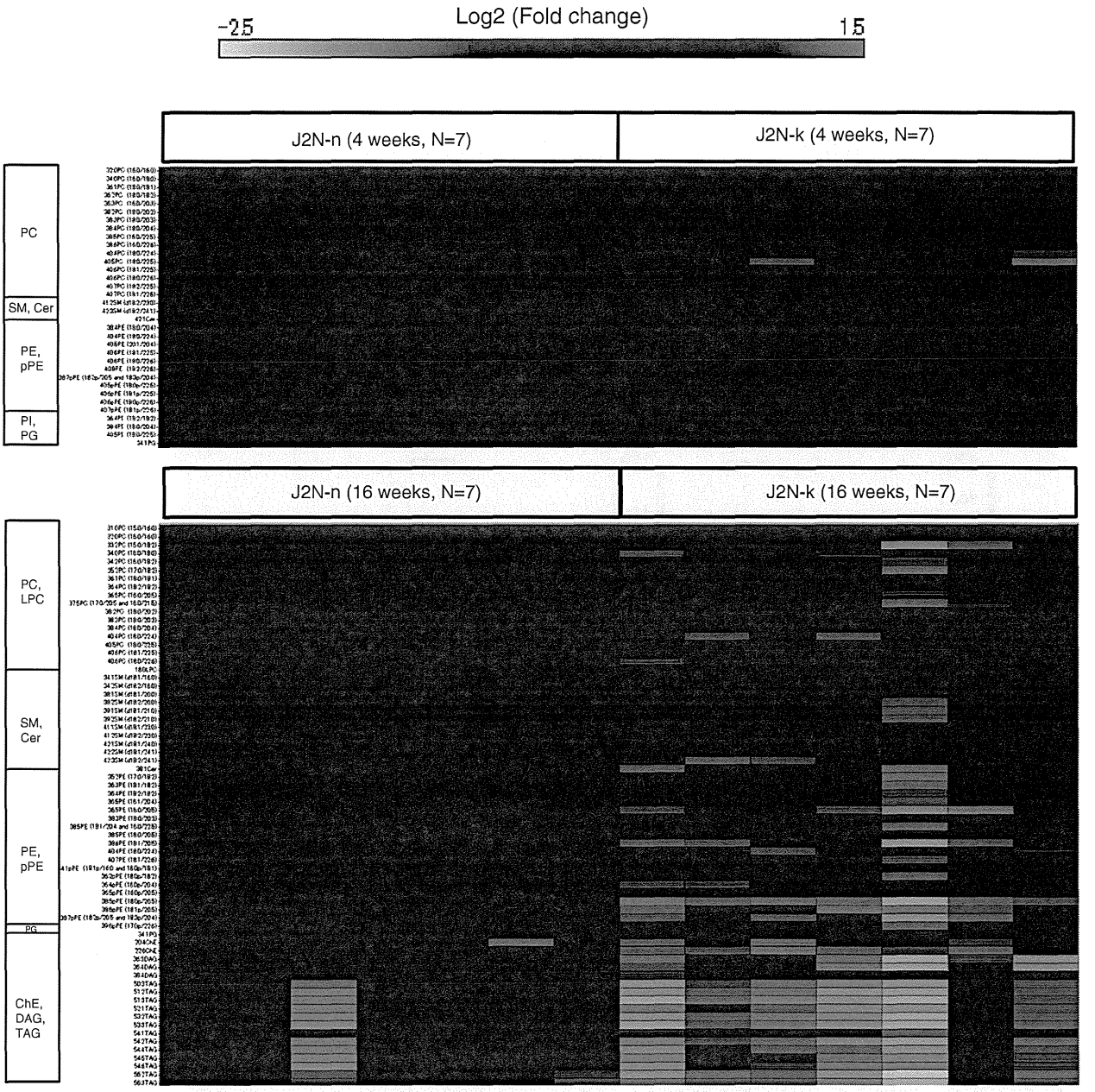

Fig. 5. Heatmap showing relative quantification of lipid metabolites identified in myocardial tissue from J2N-n and J2N-k hamsters ($n=7$ in all groups). Thirty-four (at 4 weeks) and sixty-eight (at 16 weeks) lipid metabolites with different levels ($p<0.01$) in J2N-n and age-matched J2N-k at each time point are shown. Data are represented by the log2 ratio of relative amounts of each metabolite in J2N-k to the mean relative amounts in J2N-n at either 4 or 16 weeks.

changed in J2N-k tissues at 16 weeks: 2 species, including 38:4DAG (1.6-fold, $p=2.4\times10^{-3}$), were increased, while another 7 species, predicted to contain mono- or di-unsaturated fatty acids such as 36:3DAG (0.4-fold, $p=2.2\times10^{-3}$), were significantly decreased.

3.8. Oxidative fatty acids levels were altered in J2N-k myocardial tissues

The levels of 3 prostaglandin (PGs)—PGE_2 (5.1-fold, $p=1.5\times10^{-2}$), PGD_2 (7.8-fold, $p=1.5\times10^{-2}$), and 6-keto-$PGF_{1\alpha}$ (stable metabolite of PGI_2; 8.1-fold, $p=4.6\times10^{-3}$)—were significantly increased in J2N-k myocardial tissue at 16 weeks, compared with J2N-n tissue (Fig. 6, Supplementary Table 4). Moreover, the levels of 12S-hydroxy-5Z; 8E; and 10E-heptadecatrienoic acid (12-HHT), a product of arachidonic acid via the cyclooxygenase pathway, were also increased (5.7-fold, $p=4.7\times10^{-2}$) in these tissues. In addition, levels of cyclooxygenase 2, an enzyme that catalyzes the rate-limiting step of these 4 metabolites, increased at 16 weeks in J2N-k tissue (Supplementary Fig. 7).

3.9. Increased oxidative stress in the DCM heart

Since previous reports, as well as our results (increase in ophthalmate levels), suggest the high oxidative stress levels at 16 weeks of J2N-k hamsters, we assessed lipid peroxidation and superoxide production by 4-HNE staining and DHE staining, respectively (Supplementary Figs. 8 and 9). Results from both staining confirmed an increased oxidative stress in the cardiac tissue of 16-week-old J2N-k hamsters.

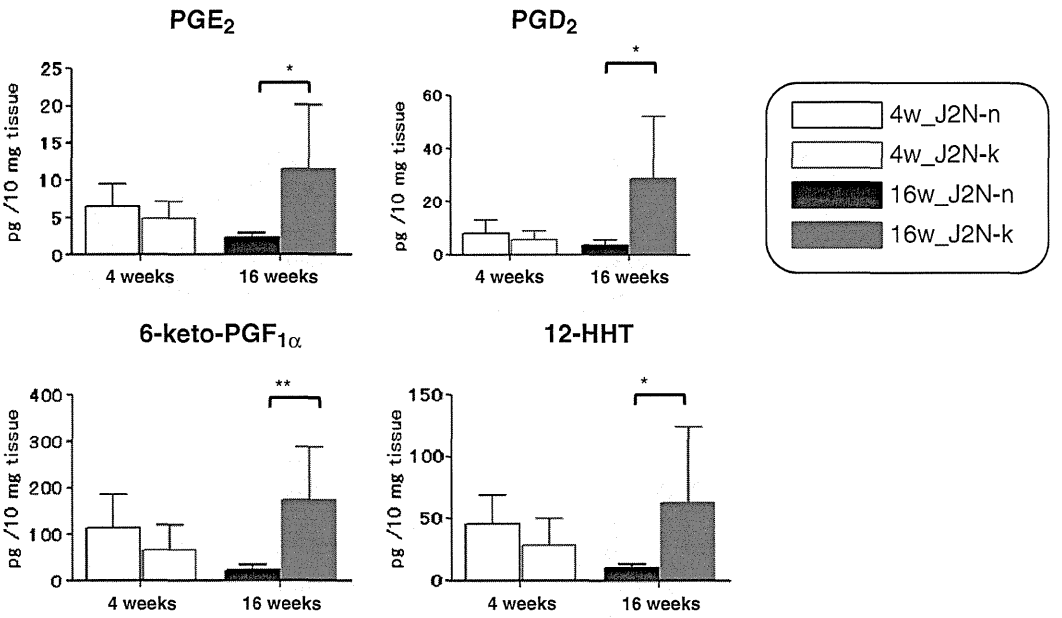

Fig. 6. Levels of 4 eicosanoids in the left ventricular tissues of 4- and 16-week-old J2N-k and J2N-n hamsters. The error bars represent mean ± SD values ($n = 7$). *$p<0.05$, **$p<0.01$, and *$p<0.001$.

4. Discussion

We performed global metabolomic analysis on myocardial tissues from J2N-k cardiomyopathic hamsters, which were found to have significantly different profiles of charged and lipid metabolites from those of J2N-n normal controls. In general, mild edema could be seen in the heart with DCM, and cardiomyocyte protein concentrations in 16-week-old J2N-k hamsters (but not 4-week-old hamsters) decreased by 9.5% compared with the J2N-n line at the same age (data not shown). However, this difference did not have a large impact on the variation in metabolite levels between J2N-k and J2N-n hamsters, and the metabolomic results were shown per tissue weights.

Analysis of charged metabolites showed significant reductions in the levels of glycolysis and TCA cycle metabolites in J2N-k myocardial tissues as compared with those of J2N-n at 16 weeks (symptomatic phase; Fig. 2). In addition to these pathways, the creatine kinase pathway also supplies energy to the heart and maintains ATP levels by the rapid transfer of high-energy phosphoryl groups from phosphocreatine to ADP. Creatine and creatinine (degradation products of phosphocreatine) levels in J2N-k symptomatic phase tissues were significantly lower than those in age-matched controls (Supplementary Table 2). It has been reported that creatine levels are attenuated in heart tissue from dystrophin-deficient *mdx* mice [19] and that creatine levels reflect the severity of heart failure in patients with DCM [20]. In addition, carnitine levels are also significantly decreased in J2N-k tissues at 16 weeks (Supplementary Table 2). Since carnitines are used for transporting fatty acids from the cytosol into the mitochondria, the availability of fatty acids for β-oxidation may be reduced in J2N-k hamsters. This supports our finding that acetyl CoA levels are considerably decreased in J2N-k tissue (ratio of 0.3 at 16 weeks, Supplementary Table 2). A recent paper also reported that Bio-TO2 cardiomyopathic hamster hearts showed reduced activity of pyruvate dehydrogenase [21], which catalyzes acetyl CoA production. These findings suggest that decreased energy production occurs in DCM hearts, resulting in reduced cardiac pumping. Further studies, such as flux analysis, are needed to validate these assumptions.

A mild reduction in GSH levels and a considerable loss of its precursor, γ-Glu-Cys in the glutathione biosynthesis pathway, were observed in J2N-k tissues at 16 weeks. In contrast, mild increases at 4 weeks and considerable increases at 16 weeks were observed for levels of ophthalmate and its precursor, 2-AB in J2N-k tissue (Fig. 3). Ophthalmate is synthesized by the same enzymes as those for GSH, but it contains 2-AB instead of cysteine [10]. Although the cysteine levels in myocardial tissue extracts were below the detection limit, the GSH synthesis pathway appeared to be upregulated based on the increased levels of its components methionine and SAH. Instead of cysteine, our data suggests that the upregulated GSH synthesis pathway uses 2-AB for ophthalmate production. This is supported by changes in the levels of other GSH and ophthalmate synthesis components: glycine levels significantly increased and glutamine (a glutamate precursor) levels decreased. We also observed increased levels of hypotaurine at both 4 and 16 weeks (Fig. 3). Unlike taurine, hypotaurine has antioxidant activity that effectively scavenges hydroxyl radicals and hypochlorous acid moieties [22]. These findings suggest that metabolic changes are initiated to counteract the increased oxidative stress observed in DCM heart tissues as confirmed in Supplementary Figs. 8 and 9.

Significant decreases in the urea cycle metabolites, arginine, argininosuccinate, and citrulline, were observed in myocardial tissues of 16-week-old J2N-k hamsters as compared to J2N-n hamsters (Fig. 4). Reductions in arginine and citrulline levels suggest a reduction in nitric oxide (NO) production by nitric oxide synthase. This is consistent with the report that NO concentrations in coronary circulation were lower in DCM patients as compared to control human subjects [23]. In contrast, increased conversion of arginine to ornithine suggests that the high arginase activity in 16-week-old J2N-k hamsters can modulate NO synthesis by limiting arginine availability for NO synthesis. NO is critical for coupling cardiac excitation-contraction by modulating Ca^{2+} homeostasis [24], suggesting its possible relation to DCM.

A recent study found that changes in lipid homeostasis contribute to the development of various cardiomyopathies [25]. In particular, dysregulation of membrane phospholipid homeostasis alters the interaction of membrane-associated protein complexes that modulate cell signaling and myocardial metabolism [26]. At the presymptomatic phase (4 weeks), we observed increased levels of PC containing unsaturated

(especially polyunsaturated) fatty acids and PE/pPE with 22:5 or 22:6 in J2N-k myocardial tissues (Fig. 5; Supplementary Table 3). In the symptomatic phase, significant decreases in PC containing linoleic acid (18:2) and many PE and pPE species, especially those containing 18:2 and/or EPA (20: 5), were observed in J2N-k hamsters. A significant accumulation of ethanolamine phosphate (1.5-fold, $p = 8.7 \times 10^{-6}$) in J2N-k tissues (Supplemental Table 2 and Fig. 1) suggests that function of the PE biosynthetic enzyme, ethanolaminephosphotransferase, may be impaired in the symptomatic phase tissues. Altered levels of the PC and PE species suggest that membrane perturbations, such as fluidity, are probably important for DCM pathology. Consistent with our results, linoleic acid (18:2) content in PC was reported to be significantly decreased in the myocardium of cardiomyopathic BIO 14.6 hamsters during the development of congestive heart failure [27]. Increased PC content (observed at 4 weeks in this study) was reported to inhibit Ca^{2+}-ATPase (SERCA) activity [28], which was indeed decreased in J2N-k cardiomyopathic hamsters [29]. Our data also show that some LPC species were significantly increased at the DCM symptomatic phase. LPCs increase the intracellular calcium concentration $[Ca^{2+}]_i$ by modulating the activities of the cardiac sarcolemmal membrane ion transporters such as SERCA [30], which may compensate for decreased contractile function. These findings suggest that contractile dysfunction in J2N-k myocardial tissue is partly attributable to aberrant PL metabolism.

At 16 weeks, J2N-k myocardial tissues exhibited altered levels of SMs and Cers of various acyl chain lengths (C16–C24; Fig. 5, Supplementary Table 3), suggesting that specific Cer signaling pathways are activated in DCM. For example, levels of Cer containing palmitic acid (16:0), such as 34:1Cer, were augmented in J2N-k tissue at 16 weeks. As 34:1Cer is a major Cer species and is known to be elevated during apoptosis induced by various agents [31]; it is possible that the apoptosis pathway is triggered in the symptomatic phase. The activation of the apoptotic pathway was reported in proteomic analysis of a phospholamban-mutated DCM mouse model [32].

The PCA of TAGs and ChEs revealed only a modest discrimination between J2N-k and J2N-n tissues both at 4 and 16 weeks (Supplementary Fig. 6B), suggesting wide within-group variations. Nevertheless, remarkable reductions were observed in several major TAG species in J2N-k tissues at 16 weeks (Fig. 5, Supplementary Table 3). TAG is stored in cytosolic lipid droplets within cardiomyocytes and ensures a continuous fatty acid supply for mitochondrial oxidation [33]. Therefore, TAG reductions suggest that heart tissue cannot secure enough energy from fatty acid oxidation, thereby leading to impaired function. Consistent with our observations, fatty acid utilization and oxidation were found to be lower in patients with idiopathic DCM than in normal controls [34]. In addition, DAGs (such as 34:2DAG and 36:3DAG) producing TAGs by diacylglycerol acyltransferase were also significantly decreased at 16 weeks (Supplementary Table 3). We observed decreased levels of glycerol-3-phosphate (a precursor of DAG and TAG, Supplementary Table 2) in J2N-k at 16 weeks, which is consistent with our lipid metabolite data.

The eicosanoids, PGE_2, PGD_2, 6-keto-$PGF_{1\alpha}$, and 12-HHT, produced by the COX pathway, were significantly (more than 5-fold) increased in J2N-k tissues at 16 weeks (Fig. 6). Although eicosanoids are generally thought to contribute to inflammatory responses associated with myocardial dysfunction, recent studies have showed that they may also have a cardioprotective role. For example, increased PGE_2 production protects the heart from ischemia-reperfusion injury via PGE_2 receptors 3 (EP3) and 4 (EP4) [35,36]. Furthermore, mice with cardiac-specific EP4 knockout display a DCM-like phenotype [37]. Elevated PGE_2 production may therefore counteract DCM pathophysiology in J2N-k hamsters. In the DCM transgenic mouse model (Tgalphaq*44 mice overexpressing the activated Galphaq protein), elevated levels of PGI_2, the active precursor of 6-keto-$PGF_{1\alpha}$, compensated for reduced NO-dependent coronary vasodilatation due to endothelial dysfunction during late-stage heart failure [38]. PGI_2 also exerted protective effects on cardiomyocytes during cardiac ischemia-reperfusion injury [39]. Elevation of at least some of these 4 eicosanoids may therefore counteract DCM pathophysiology in the J2N-k model.

5. Conclusions

We performed global metabolomic analysis on left ventricular heart tissues from hamsters with hereditary DCM. In the symptomatic phase, the levels of the most significantly altered charged metabolites are mapped to energy metabolism, the glutathione biosynthesis pathway, and the urea cycle. Specifically, a mild reduction in GSH and a compensatory increase in ophthalmate suggested that increased oxidative stress played a role in DCM pathogenesis; this was later confirmed by 4-HNE and DHE histochemistry. Regarding lipid metabolites, disturbances in membrane phospholipid homeostasis (changes in PC and PE species levels) began even at the presymptomatic phase. The potential involvement of specific eicosanoids in the cardioprotective pathways was suggested by increased levels of these metabolites during the symptomatic phase. Further investigation is required to determine how changes in the concentration of the metabolites identified in this study contribute to cardiac dysfunction in DCM. However, our work does provide insight into the mechanisms involved in DCM pathogenesis and may lead to the identification of new targets for therapeutic intervention or diagnosis.

Abbreviations

2-AB	2-aminobutyrate
4-HNE	4-hydroxynonenal
CE	capillary electrophoresis
Cer	ceramide
ChE	cholesterol ester
DAG	diacylglycerols
DCM	dilated cardiomyopathy
DGC	dystrophin-glycoprotein complex
DHA	docosahexaenoic acid
DHE	dihydroethidium,
EPA	eicosapentaenoic acid
GSH	glutathione
HHT	heptadecatrienoic acid
IS	internal standard
LC	liquid chromatography
LPC	lysoPC
MS	mass spectrometry
NO	nitric oxide
PC	phosphatidylcholine
PCA	principal component analysis
PE	phosphatidylethanolamine
PG	prostaglandin;
PL	phospholipid
pPE	plasmalogen PE
RT	retention time
SM	sphingomyelin
TAG	triacylglycerol
TCA	tricarboxylic acid
TOF	time-of-flight

Supplementary data to this article can be found online at http://dx.doi.org/10.1016/j.yjmcc.2013.02.008.

Funding

This work was supported by the Advanced Research for Products Mining Programme [grant number 10-45] from the National Institute of Biomedical Innovation of Japan to NM, TS, and YS.

Disclosures

None.

References

[1] Luk A, Ahn E, Soor GS, Butany J. Dilated cardiomyopathy: a review. J Clin Pathol 2009;62:219–25.
[2] Tigen K, Cevik C. Beta-blockers in the treatment of dilated cardiomyopathy: which is the best? Curr Pharm Des 2010;16:2866–71.
[3] Takeda N. Cardiomyopathy: molecular and immunological aspects (review). Int J Mol Med 2003;11:13–6.
[4] Seidman JG, Seidman C. The genetic basis for cardiomyopathy: from mutation identification to mechanistic paradigms. Cell 2001;104:557–67.
[5] Campbell KP. Three muscular dystrophies: loss of cytoskeleton-extracellular matrix linkage. Cell 1995;80:675–9.
[6] Yucel D, Aydogdu S, Senes M, Topkaya BC, Nebioglu S. Evidence of increased oxidative stress by simple measurements in patients with dilated cardiomyopathy. Scand J Clin Lab Invest 2002;62:463–8.
[7] Demirbag R, Yilmaz R, Erel O, Gultekin U, Asci D, Elbasan Z. The relationship between potency of oxidative stress and severity of dilated cardiomyopathy. Can J Cardiol 2005;21:851–5.
[8] Baumer AT, Flesch M, Wang X, Shen Q, Feuerstein GZ, Bohm M. Antioxidative enzymes in human hearts with idiopathic dilated cardiomyopathy. J Mol Cell Cardiol 2000;32:121–30.
[9] Mitsuhashi S, Saito N, Watano K, Igarashi K, Tagami S, Shima H, et al. Defect of delta-sarcoglycan gene is responsible for development of dilated cardiomyopathy of a novel hamster strain, J2N-k: calcineurin/PP2B activity in the heart of J2N-k hamster. J Biochem 2003;134:269–76.
[10] Soga T, Baran R, Suematsu M, Ueno Y, Ikeda S, Sakurakawa T, et al. Differential metabolomics reveals ophthalmic acid as an oxidative stress biomarker indicating hepatic glutathione consumption. J Biol Chem 2006;281:16768–76.
[11] Nakamura K, Kusano K, Nakamura Y, Kakishita M, Ohta K, Nagase S, et al. Carvedilol decreases elevated oxidative stress in human failing myocardium. Circulation 2002;105:2867–71.
[12] Fujii T, Onohara N, Maruyama Y, Tanabe S, Kobayashi H, Fukutomi M, et al. Galpha12/13-mediated production of reactive oxygen species is critical for angiotensin receptor-induced NFAT activation in cardiac fibroblasts. J Biol Chem 2005;280:23041–7.
[13] Soga T, Igarashi K, Ito C, Mizobuchi K, Zimmermann HP, Tomita M. Metabolomic profiling of anionic metabolites by capillary electrophoresis mass spectrometry. Anal Chem 2009;81:6165–74.
[14] Soga T, Heiger DN. Amino acid analysis by capillary electrophoresis electrospray ionization mass spectrometry. Anal Chem 2000;72:1236–41.
[15] Bligh EG, Dyer WJ. A rapid method of total lipid extraction and purification. Can J Biochem Physiol 1959;37:911–7.
[16] Taguchi R, Ishikawa M. Precise and global identification of phospholipid molecular species by an Orbitrap mass spectrometer and automated search engine Lipid Search. J Chromatogr A 2010;1217:4229–39.
[17] Sugimoto M, Wong DT, Hirayama A, Soga T, Tomita M. Capillary electrophoresis mass spectrometry-based saliva metabolomics identified oral, breast and pancreatic cancer-specific profiles. Metabolomics 2010;6:78–95.
[18] Ono M, Shitashige M, Honda K, Isobe T, Kuwabara H, Matsuzuki H, et al. Label-free quantitative proteomics using large peptide data sets generated by nanoflow liquid chromatography and mass spectrometry. Mol Cell Proteomics 2006;5:1338–47.
[19] Gulston MK, Rubtsov DV, Atherton HJ, Clarke K, Davies KE, Lilley KS, et al. A combined metabolomic and proteomic investigation of the effects of a failure to express dystrophin in the mouse heart. J Proteome Res 2008;7:2069–77.
[20] Nakae I, Mitsunami K, Yoshino T, Yoshino T, Omura T, Tsutamoto T, et al. Clinical features of myocardial triglyceride in different types of cardiomyopathy assessed by proton magnetic resonance spectroscopy: comparison with myocardial creatine. J Card Fail 2010;16:812–22.
[21] Missihoun C, Zisa D, Shabbir A, Lin H, Lee T. Myocardial oxidative stress, osteogenic phenotype, and energy metabolism are differentially involved in the initiation and early progression of delta-sarcoglycan-null cardiomyopathy. Mol Cell Biochem 2009;321:45–52.
[22] Aruoma OI, Halliwell B, Hoey BM, Butler J. The antioxidant action of taurine, hypotaurine and their metabolic precursors. Biochem J 1988;256:251–5.
[23] Takarada S, Imanishi T, Goto M, Mochizuki S, Ikejima H, Tsujioka H, et al. First evaluation of real-time nitric oxide changes in the coronary circulation in patients with non-ischaemic dilated cardiomyopathy using a catheter-type sensor. Eur Heart J 2010;31:2862–70.
[24] Zima AV, Blatter LA. Redox regulation of cardiac calcium channels and transporters. Cardiovasc Res 2006;71:310–21.
[25] Wende AR, Abel ED. Lipotoxicity in the heart. Biochim Biophys Acta 1801;2010: 311–9.
[26] Jenkins CM, Cedars A, Gross RW. Eicosanoid signalling pathways in the heart. Cardiovasc Res 2009;82:240–9.
[27] Okumura K, Yamada Y, Kondo J, Hashimoto H, Ito T, Kitoh J. Decreased 1,2-diacylglycerol levels in myopathic hamster hearts during the development of heart failure. J Mol Cell Cardiol 1991;23:409–16.
[28] Fu S, Yang L, Li P, Hofmann O, Dicker L, Hide W, et al. Aberrant lipid metabolism disrupts calcium homeostasis causing liver endoplasmic reticulum stress in obesity. Nature 2011;473:528–31.
[29] Babick AP, Cantor EJ, Babick JT, Takeda N, Dhalla NS, Netticadan T. Cardiac contractile dysfunction in J2N-k cardiomyopathic hamsters is associated with impaired SR function and regulation. Am J Physiol Cell Physiol 2004;287: C1202–8.
[30] Yu L, Netticadan T, Xu YJ, Panagia V, Dhalla NS. Mechanisms of lysophosphatidylcholine-induced increase in intracellular calcium in rat cardiomyocytes. J Pharmacol Exp Ther 1998;286:1–8.
[31] Pewzner-Jung Y, Ben-Dor S, Futerman AH. When do Lasses (longevity assurance genes) become CerS (ceramide synthases)?: insights into the regulation of ceramide synthesis. J Biol Chem 2006;281:25001–5.
[32] Gramolini AO, Kislinger T, Alikhani-Koopaei R, Fong V, Thompson NJ, Isserlin R, et al. Comparative proteomics profiling of a phospholamban mutant mouse model of dilated cardiomyopathy reveals progressive intracellular stress responses. Mol Cell Proteomics 2008;7:519–33.
[33] Banke NH, Wende AR, Leone TC, O'Donnell JM, Abel ED, Kelly DP, et al. Preferential oxidation of triacylglyceride-derived fatty acids in heart is augmented by the nuclear receptor PPARalpha. Circ Res 2010;107:233–41.
[34] Dávila-Román VG, Vedala G, Herrero P, de las Fuentes L, Rogers JG, Kelly DP, et al. Altered myocardial fatty acid and glucose metabolism in idiopathic dilated cardiomyopathy. J Am Coll Cardiol 2002;40:271–7.
[35] Martin M, Meyer-Kirchrath J, Kaber G, Jacoby C, Flögel U, Schrader J, et al. Cardiospecific overexpression of the prostaglandin EP3 receptor attenuates ischemia-induced myocardial injury. Circulation 2005;112:400–6.
[36] Xiao CY, Yuhki K, Hara A, Fujino T, Kuriyama S, Yamada T, et al. Prostaglandin E2 protects the heart from ischemia-reperfusion injury via its receptor subtype EP4. Circulation 2004;109:2462–8.
[37] Harding P, Yang XP, Yang J, Shesely E, He Q, LaPointe MC. Gene expression profiling of dilated cardiomyopathy in older male EP4 knockout mice. Am J Physiol Heart Circ Physiol 2010;298:H623–32.
[38] Drelicharz L, Kozlovski V, Skorka T, Heinze-Paluchowska S, Jasinski A, Gebska A, et al. NO and PGI(2) in coronary endothelial dysfunction in transgenic mice with dilated cardiomyopathy. Basic Res Cardiol 2008;103:417–30.
[39] Xiao CY, Hara A, Yuhki K, Fujino T, Ma H, Okada Y, et al. Roles of prostaglandin I(2) and thromboxane A(2) in cardiac ischemia-reperfusion injury: a study using mice lacking their respective receptors. Circulation 2001;104:2210–25.

Cardiovascular Research (2013) **99**, 760–768
doi:10.1093/cvr/cvt163

Blockade of sarcolemmal TRPV2 accumulation inhibits progression of dilated cardiomyopathy

Yuko Iwata[1]*, Hitomi Ohtake[1], Osamu Suzuki[2], Junichiro Matsuda[2], Kazuo Komamura[3], and Shigeo Wakabayashi[1]

[1]Department of Molecular Physiology, National Cerebral and Cardiovascular Center Research Institute, Fujishiro-dai 5-7-1, Suita, Osaka 565-8565, Japan; [2]Laboratory of Animal Models for Human Diseases, National Institute of Biomedical Innovation, Ibaraki, Osaka 567-0085, Japan; and [3]Department of Clinical Pharmacology and Pharmacogenomics, Graduate School of Pharmaceutical Science, Osaka University, Suita, Osaka 565-0871, Japan

Received 23 January 2013; revised 1 June 2013; accepted 14 June 2013; online publish-ahead-of-print 19 June 2013

Time for primary review: 10 days

Aims Dilated cardiomyopathy (DCM) is a severe disorder defined by ventricular dilation and contractile dysfunction. Abnormal Ca^{2+} handling is hypothesized to play a critical pathological role in DCM progression. The transient receptor potential vanilloid 2 (TRPV2) has been previously suggested as a candidate pathway for enhanced Ca^{2+} entry. Here, we examined the sarcolemmal accumulation of TRPV2 in various heart-failure model animals and DCM patients, and assessed whether presently available inhibitory tools against TRPV2 ameliorate DCM symptoms.

Methods and results Immunological and cell physiological analyses revealed that TRPV2 is highly concentrated and activated in the ventricular sarcolemma of DCM patients and three animal models—δ-sarcoglycan-deficient hamsters (J2N-k), transgenic mice over-expressing sialytransferase (4C30), and doxorubicin (DOX)-induced DCM mice. Over-expression of the amino-terminal (NT) domain of TRPV2 could block the plasma membrane accumulation and influx of Ca^{2+} via TRPV2. Transgenic (Tg) or adenoviral expression of the NT domain in DCM animals caused effective removal of sarcolemmal TRPV2 along with reduction in the phosphorylation of calmodulin-dependent protein kinase II (CaMKII) and reactive oxygen species (ROS) production, which were activated in DCM; further, it prevented ventricular dilation and fibrosis, ameliorated contractile dysfunction in DCM, and improved survival of the affected animals. The TRPV2 inhibitor tranilast markedly suppressed DCM progression.

Conclusion Sarcolemmal TRPV2 accumulation appears to have considerable pathological impact on DCM progression, and blockade of this channel may be a promising therapeutic strategy for treating advanced heart failure.

Keywords Dilated cardiomyopathy • Heart failure • Therapeutic tool • Ca^{2+}-permeable channel • DOX-induced cardiomyopathy

1. Introduction

Dilated cardiomyopathy (DCM) is a severe disorder defined by ventricular dilation and cardiac dysfunction.[1–3] Although a considerable proportion of DCM cases develop because of inflammatory, metabolic, or toxic effects from medications, 30–48% of DCM cases are caused by genetic mutations.[4] Some affected genes encode sarcomeric or cytoskeletal proteins, including the components of the dystrophin–glycoprotein complex (DGC).[5,6] For example, δ-sarcoglycan-deficient hamsters (J2N-k) provide an animal model of human limb-girdle muscular dystrophy-associated DCM. However, little information is available regarding the pathways by which heterogeneous genetic defects and/or various causes lead to DCM symptoms.

The calcium ion (Ca^{2+}) plays a pivotal role in the pathogenesis of cardiac disease.[7,8] Ca^{2+}-handling abnormalities have been found in various forms of heart failure, including DCM.[9–11]

Further Ca^{2+}-permeable transient receptor potential (TRP) channels have recently been recognized as key molecules in pathological cardiac hypertrophy and heart failure.[12–14] We have previously reported that cardiac-specific over-expression of TRP vanilloid 2 (TRPV2) results in DCM with outstanding ventricular dilation,[15] suggesting that chronic elevation in cytosolic Ca^{2+} concentrations ($[Ca^{2+}]_i$) is critical in DCM pathogenesis. However, it is unclear whether TRPV2 activity is a risk factor for DCM in humans as well as animals and whether TRPV2 inhibition can be beneficial against DCM progression, because of the limited number of methods for specific TRPV2 inhibition.

* Corresponding author. Tel: +81 6833 5012; fax: +81 6 6835 5314, Email: yukoiwat@ri.ncvc.go.jp

Therefore, we examined the role of TRPV2 in DCM. We also assessed the effect of TRPV2 blockades on cardiac dysfunction and DCM progression in several animal models.

2. Methods

Detailed methods are available in the Supplementary material online.

2.1 Molecular biology

All plasmid construction involving TRPV2 was carried out via a PCR-based strategy using the full-length mouse TRPV2 cDNA cloned into the pIRES expression vector (Invitrogen). Restriction enzyme-digested PCR products corresponding to the amino-terminal (NT) (amino acids (aa) 1–387) and carboxyl-terminal (CT) (aa 633–756) domains of TRPV2 were cloned into the p3Xflag-CMV-14 expression vector (Sigma-Aldrich). For adenoviral gene transfer, we inserted the haemagglutinin (HA)-tagged NT domain of TRPV2 (amino acids 1–387) cDNA into the pAd/CMV/V5-DEST viral vector (Invitrogen).

2.2 Animals and drug administration

DCM mice (4C30) were produced as described previously.[16] Heart-specific NT-transgenic (Tg) mice were generated from C57BL/6J mice according to the standard procedures.[15]

J2N-k hamsters, and age-matched normal controls (J2N-n) were purchased from Japan SLC. J2N-k hamsters were orally administered tranilast for 14 days at a dose of 30 or 300 mg/kg per day. In the DOX experiment, wild-type (WT) and NT-Tg mice were chronically treated with either phosphate-buffered saline (PBS; control) or doxorubicin (DOX) (Pfizer) by four intraperitoneal (i.p) injections (d 0, 2, 4, and 6) at a dose of 4 mg/kg (cumulative dose totalling 16 mg/kg). All animal experiments were performed in accordance with the Guidelines for Animal Experimentation of the National Cerebral and Cardiovascular Center (NCVC), and procedures were carried out in accordance with the Guide for the Care and Use of Laboratory Animals published by the US National Institutes of Health (NIH; NIH Publication, 8th Edition, 2011).

2.3 Histology, immunoblotting, and immunohistochemistry

Animals were anaesthetized with 5% isoflurane in an anaesthesia chamber until unresponsive to nose pinch, and the heart was harvested for

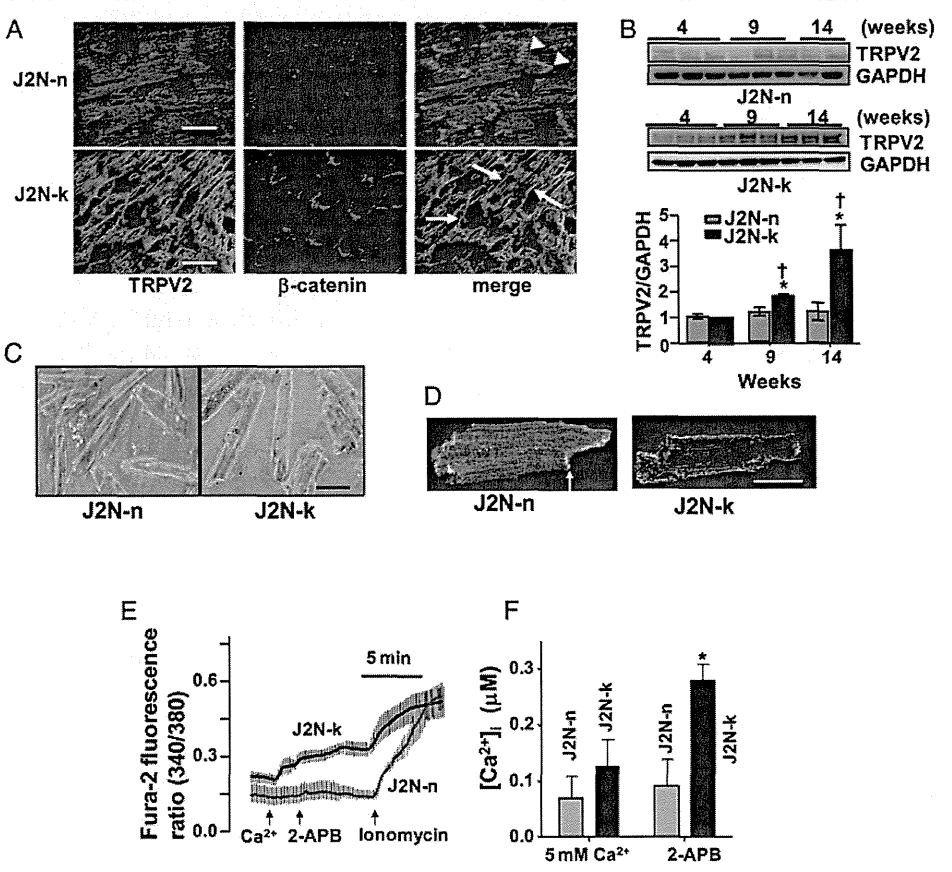

Figure 1 TRPV2 accumulation and activation in the sarcolemma of cardiomyopathic hearts. (*A*) Immunohistochemical analysis of frozen ventricular sections from 8-week-old J2N-n and J2N-k hamsters with TRPV2 and β-catenin antibodies. β-catenin-positive intercalated discs or sarcolemmal regions are shown by arrowheads or arrows, respectively. Scale bar: 50 μm. (*B*) Immunoblots (40 μg/lane) of TRPV2-immunostained cardiac muscles. Age-dependent increases in the expression level of TRPV2 are observed. The data represent mean ± SD values ($n = 4–6$ hamsters/group); $^*P < 0.05$ vs. 4 weeks, $^\dagger P < 0.05$ vs. J2N-n. (*C*) Phase-contrast micrographs of freshly isolated ventricular cardiomyocytes. Scale bar: 30 μm. (*D*) Confocal micrographs of TRPV2-immunostained isolated cardiomyocytes. TRPV2 is extensively localized to the sarcolemma in J2N-k cells but to the intracellular compartment and intercalated disc (arrow) in J2N-n cells. Scale bar: 30 μm. (*E*) Intracellular Ca^{2+} increase in response to extracellular Ca^{2+} (5 mM) and 2-APB (500 μM) in cardiomyocytes loaded with fura-2. (*F*) Intracellular Ca^{2+} concentration calculated from three independent experiments. The data represent mean ± SD values ($n = 7–10$ cardiomyocytes/group); $^*P < 0.05$.

biochemical assays. These experiments were conducted as described previously.[15,17,18]

2.4 Echocardiography

Cardiac function was evaluated by echocardiography using a Hewlett Packard Sonos 5500 ultrasound system with a 12-MHz transducer and M-mode imaging. Animals were sedated with tribromoethanol [i.p, 350 mg/kg of body weight (BW)] during the procedure.

2.5 Cardiomyocyte isolation and $[Ca^{2+}]_i$ measurement

Single-ventricular cardiomyocytes were freshly isolated from adult mouse and hamster hearts using standard enzymatic techniques.[19] The $[Ca^{2+}]_i$ was measured at room temperature via a ratiometric fluorescence method using fura-2 or indo-1 acetoxymethyl ester.[17,19]

2.6 Human tissues

Cardiac tissue samples were obtained from patients with DCM (Supplementary material online, *Table*). Written informed consent was obtained from all living patients, and the experiments on human tissues were approved by the Institutional Review Board of the NCVC. The investigation conforms to the principles of the Declaration of Helsinki.

2.7 Statistical analysis

We used an unpaired Student's *t*-test and one-way ANOVA followed by Dunnett's test for statistical analysis. $P < 0.05$ indicates statistical significance.

3. Results

3.1 TRPV2 is concentrated and activated in cardiomyopathic hearts

To study the role of TRPV2 in DCM, we first examined the expression and subcellular distribution of TRPV2 in the ventricles of δ-sarcoglycan-deficient (J2N-k) hamsters. In their normal control counterparts (J2N-n, 8-week-old hamsters), most of the TRPV2 expression was observed in the cell interior and in regions co-stained with the intercalated disc marker β-catenin (*Figure 1A*). In contrast, age-matched J2N-k ventricles showed increased TRPV2 expression in the peripheral sarcolemma as well as in parts of the intercalated discs (*Figure 1A*). With disease progression, total TRPV2 expression levels gradually increased only in J2N-k ventricles (from 9-week-old hamsters; *Figure 1B*). Although apparently similar rod shapes and sizes were noted in isolated cardiomyocytes from both types of hamsters (*Figure 1C*), stronger TRPV2 surface expression was observed in J2N-k cardiomyocytes than in controls (*Figure 1D*).

In J2N-k cardiomyocytes expressing TRPV2 in the sarcolemma, a rapid and large increase in $[Ca^{2+}]_i$ was elicited by exposure to the TRPV2 channel activator 2-aminoethoxydiphenyl borate (2-APB) as well as a high-Ca^{2+} solution, whereas increases in $[Ca^{2+}]_i$ were marginal in control J2N-n cardiomyocytes (*Figure 1E* and *F*); this increase was inhibited by the TRPV channel antagonist ruthenium red (data not shown). Although TRPV1–3 are known to be activated by 2-APB,[20] cardiac tissues did not show detectable TRPV1 or TRPV3 expression (data not shown). Furthermore, although 2-APB is known to inhibit the intracellular Ca^{2+}-release channel inositol 1, 4, 5-trisphosphate receptor (IP_3R) and other TRP channel family proteins,[21] we saw an

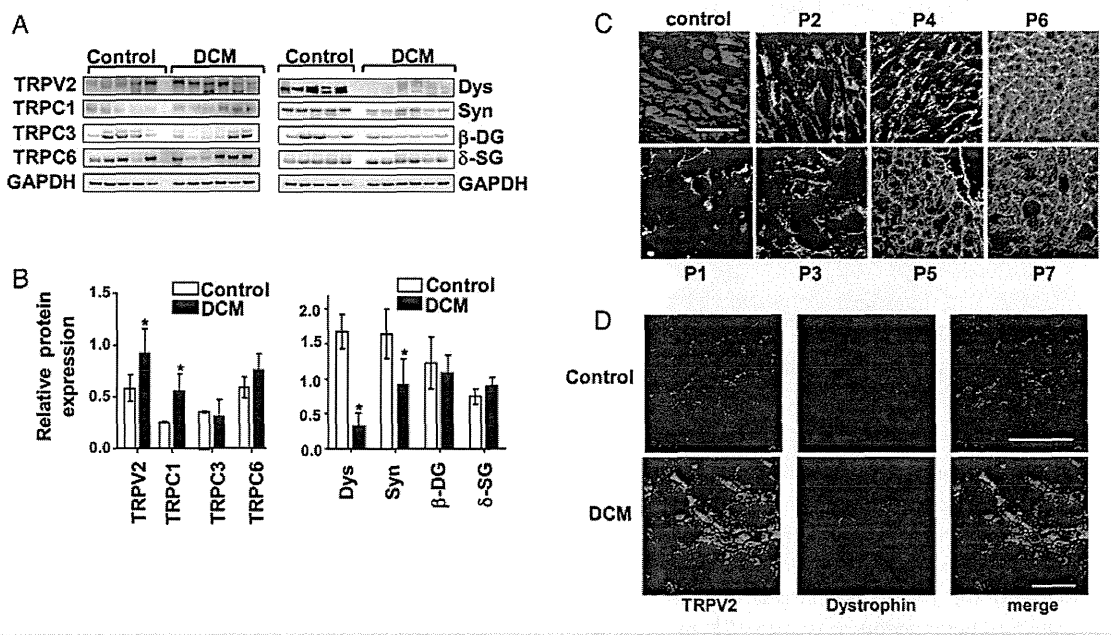

Figure 2 Sarcolemmal TRPV2 accumulation in human DCM. (*A*) Representative immunoblot data of human heart homogenates. Controls and DCM patients; dys, dystrophin; syn, syntrophin; DG, dystroglycan; SG, sarcoglycan; TRPC, transient receptor potential canonical. (*B*) Protein expression levels relative to GAPDH expression in control (white bars) and patient (black bars) samples. The data represent mean ± SD values from four4 independent experiments ($n = 5–7$ samples/group); *$P < 0.05$. (*C*) TRPV2 immunostaining of frozen human ventricular sections. P1–P7 (Supplementary material online, *Table S1*). Scale bar: 100 μm. (*D*) Ventricular sections from control and DCM patient were co-immunostained with TRPV2 and dystrophin. Note the surface localizsation of TRPV2 and reduced number of dystrophin-positive myocytes in DCM. Scale bar: 100 μm.

increase in $[Ca^{2+}]_i$, which is why TRPV2 was considered the principal candidate involved in the 2-APB-induced $[Ca^{2+}]_i$ increase in J2N-k cardiomyocytes. In addition, we observed that 2-APB often induced abnormal Ca^{2+} elevation accompanied by loss of regular Ca^{2+}-transients under electrically stimulated conditions in J2N-k cardiomyocytes (but not in J2N-n control cardiomyocytes; unpublished observations). These data suggest that sarcolemmal TRPV2 accumulation contributes to the increased $[Ca^{2+}]_i$ levels in J2N-k cardiomyocytes.

In addition to the J2N-k hamster, other animal models with DCM display sarcolemmal accumulation of TRPV2. One such model is the 4C30 mouse, which over-expresses β-galactoside α-2,3-sialytransferase II (ST3Gal-II) and was recently developed as a model for human DCM; the other is DOX-induced DCM, a widely familiar model, although its precise mechanism of cardiotoxicity remains debatable. In hearts from these two animal models, total expression (see *Figures 4A* and *5E*) and sarcolemmal accumulation of TRPV2 (see *Figures 4B* and *5D* and Supplementary material online, *Figures S1* and *S2*) were found to be largely increased when compared with WT mice. In 4C30 mice, expression of TRP canonical (TRPC6), but not that of TRPC1 and TRPC3, was slightly increased (Supplementary material online, *Figure S3*); however, expression of α-dystroglycan and α-sarcoglycan were greatly reduced (Supplementary material online, *Figure S4*).

We next studied TRPV2 expression in ventricular samples from DCM patients (Supplementary material online, *Table S1*). TRPV2 and TRPC1 expression was significantly higher in DCM patients than in controls (*Figure 2A* and *B*), but expression of TRPC3 and TRPC6 was not significantly different. All DCM samples also exhibited reduced dystrophin and syntrophin expression levels (*Figure 2A* and *B*), suggesting that DCM is somehow linked to abnormal cytoskeletal organization. Similar to the findings in J2N-k ventricles, strong TRPV2 immunostaining was detected only in the peripheral sarcolemma of DCM cardiomyocytes (*Figure 2C*). Part of the TRPV2 expression was co-localized with the subsarcolemmal cytoskeletal protein dystrophin in human DCM ventricles, although dystrophin was detected only in a limited number of myocytes (*Figure 2D*).

3.2 Over-expression of the NT domain effectively blocks plasma membrane accumulation of TRPV2

We hypothesized that sarcolemmal TRPV2 accumulation is a common factor leading to Ca^{2+}-induced muscle degeneration in various heart diseases. Therefore, translocation of TRPV2 from the sarcolemma to the cell interior could be a promising therapeutic method. To study such 'back-translocation' of TRPV2, we used HEK293 cells, because they always recruit TRPV2 to the plasma membrane, independent of growth conditions, upon its heterologous expression (*Figure 3A*). We examined over-expression of several functional domains of TRPV2 together with full-length TRPV2 to identify the part of the TRPV2 molecule required for plasma membrane accumulation. We found that when the NT domain of TRPV2 was over-expressed, the majority of TRPV2 molecules moved from the sarcolemma to the cell interior (*Figure 3A*); such translocation was not observed with CT domain over-expression (*Figure 3A*). Consistent with this, over-expression of the NT but not the CT domain dramatically inhibited 2-APB-induced $[Ca^{2+}]_i$ increase (*Figure 3B* and *C*). Thus, the NT domain may be a useful tool for abrogating the sarcolemmal TRPV2 accumulation, thereby inhibiting the sustained increase in $[Ca^{2+}]_i$ in agonist-stimulated cells. To examine the effect of NT domain over-expression on DCM symptoms, we used 4C30 mice and DOX-induced DCM mice.

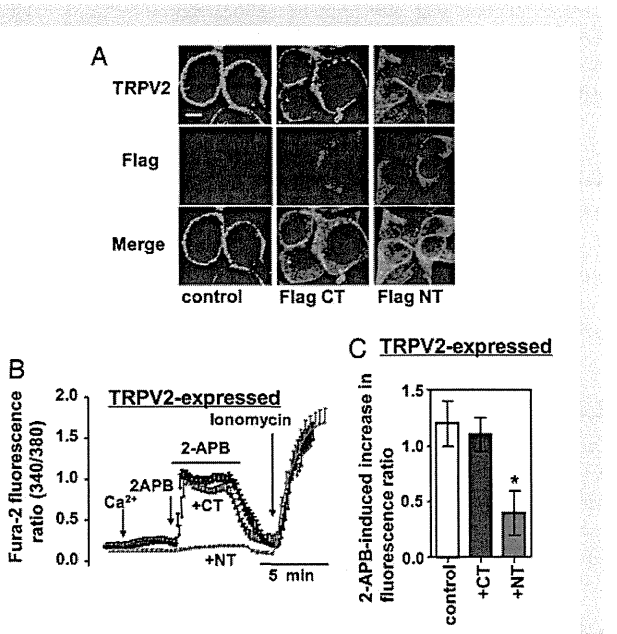

Figure 3 Over-expression of the TRPV2 NT domain blocks the surface expression of TRPV2. (*A*) HEK293 cells expressing TRPV2 were transfected with Flag-tagged CT or NT domain and immunostained with anti-TRPV2 and anti-Flag antibodies. Note that the over-expression of the NT domain reduced TRPV2 surface expression. Scale bar: 10 μm. (*B*) Intracellular Ca^{2+} increase in response to extracellular Ca^{2+} (5 mM) and 2-APB (500 μM) in cells loaded with fura-2. (*C*) The peak fura-2 ratio induced by 2-APB was summarized from three independent experiments. The data represent mean ± SD values (n = over 10 cells/group); $^*P < 0.05$.

3.3 Tg expression of the NT domain ameliorates cardiomyopathy in 4C30 mice

We generated Tg mice expressing the HA-tagged NT domain (*Figure 4A*) under the control of the α-myosin heavy chain (α-MHC) promoter. NT-Tg mice were apparently healthy as evidenced by normal heart morphology (*Figure 4C*), cardiac function (*Figure 4G* and *H*) and life span (*Figure 4I*). The NT domain was introduced into the hearts of 4C30 mice by crossing them with NT-Tg mice. Interestingly, elevated expression level of endogenous TRPV2 in 4C30 mice was decreased to control levels in 4C30/NT-Tg mice (*Figure 4A*). The exogenous NT domain was mostly localized to intercalated discs in both NT-Tg and 4C30/NT-Tg mice (*Figure 4B*). As expected, the sarcolemmal localization of TRPV2 in 4C30 mice was dramatically reduced following NT domain over-expression (4C30/NT-Tg) (*Figure 4B*), potentially leading to a reduction in sustained $[Ca^{2+}]_i$ increase. Consistent with this idea, CaMKII phosphorylation was markedly reduced in the 4C30/NT-Tg mice (*Figure 4A*). In addition, the expression level of modulatory calcineurin inhibitory protein-1 (MCIP) was increased in 4C30 mice but reduced in 4C30/NT-Tg mice (*Figure 4A*), further suggesting that blockade of TRPV2 results in a reduction in sustained $[Ca^{2+}]_i$ increase.

In 4C30 mice aged more than 120 days, we observed thinner ventricular walls and greater ventricular dilation accompanied by fibrosis (*Figure 4C*), with increased serum cardiac troponin I (cTnI; a heart

injury marker) levels (*Figure 4D*). Furthermore, reactive oxygen species (ROS) production measured by dihydroethidium (DHE) staining (*Figure 4E*) and the extent of lipid peroxidation estimated by measurement of 4-hydroxynonenal (4-HNE) adducts (*Figure 4F*) were significantly higher in the 4C30 mice, suggesting high oxidative stress in these DCM hearts. The 4C30/NT-Tg mice showed marked suppression of these symptoms (*Figure 4C–F*). Echocardiographically, the 4C30 mice showed increased left-ventricular diastolic and systolic dimensions (LVDd and LVDs, respectively), with decreased fractional shortening (FS) and ejection fractions (EF) (*Figure 4G* and *H*). However, the 4C30/NT-Tg mice had significantly improved cardiac functions. Moreover, the 4C30 mice progressively died at 200–300 days after birth, but 4C30/NT-Tg mice had a much longer life span, particularly the female mice (*Figure 4I*). We suspect that the amelioration in DCM symptoms may have resulted from the removal of endogenous TRPV2 from the sarcolemma.

3.4 Beneficial effects of NT domain over-expression in DOX-induced DCM

The effects of NT domain over-expression were next examined in DOX-induced DCM. In WT mice, DOX treatment resulted in ventricular dilation, reduced FS, and higher mortality (*Figure 5A–C*). In contrast, DOX-treated NT-Tg mice demonstrated better cardiac morphology and function and better survival (*Figure 5A–C*). Indeed, upon DOX treatment, the NT-Tg mice showed lower TRPV2 expression and sarcolemmal accumulation of TRPV2 (*Figure 5D* and *E*), demonstrating reduced CaMKII phosphorylation (*Figure 5E*) and oxidative stress (*Figure 5F* and *G*). These results suggest that TRPV2 also plays an important pathological role in non-genetic heart failure, such as DOX-induced DCM.

3.5 Adenoviral expression of the NT domain ameliorates cardiac dysfunction in J2N-k hamsters

We next addressed whether the effects of the NT domain could be seen in J2N-k cardiomyopathy following over-expression via adenoviral transfer. We injected an adenovirus carrying either β-galactosidase (β-gal; as a control) or the NT domain into the hearts of 9-week-old J2N-k hamsters, at which age sarcolemmal TRPV2 translocation and cardiac dysfunction had already been observed. At 14 days post-injection, we detected NT domain expression in the ventricles by immunoblotting with the HA antibody (*Figure 6A*). Detection of green fluorescent protein (GFP) in cardiac homogenates (*Figure 6A*) and sections (*Figure 6B*) confirmed that the adenoviral vector had reached the

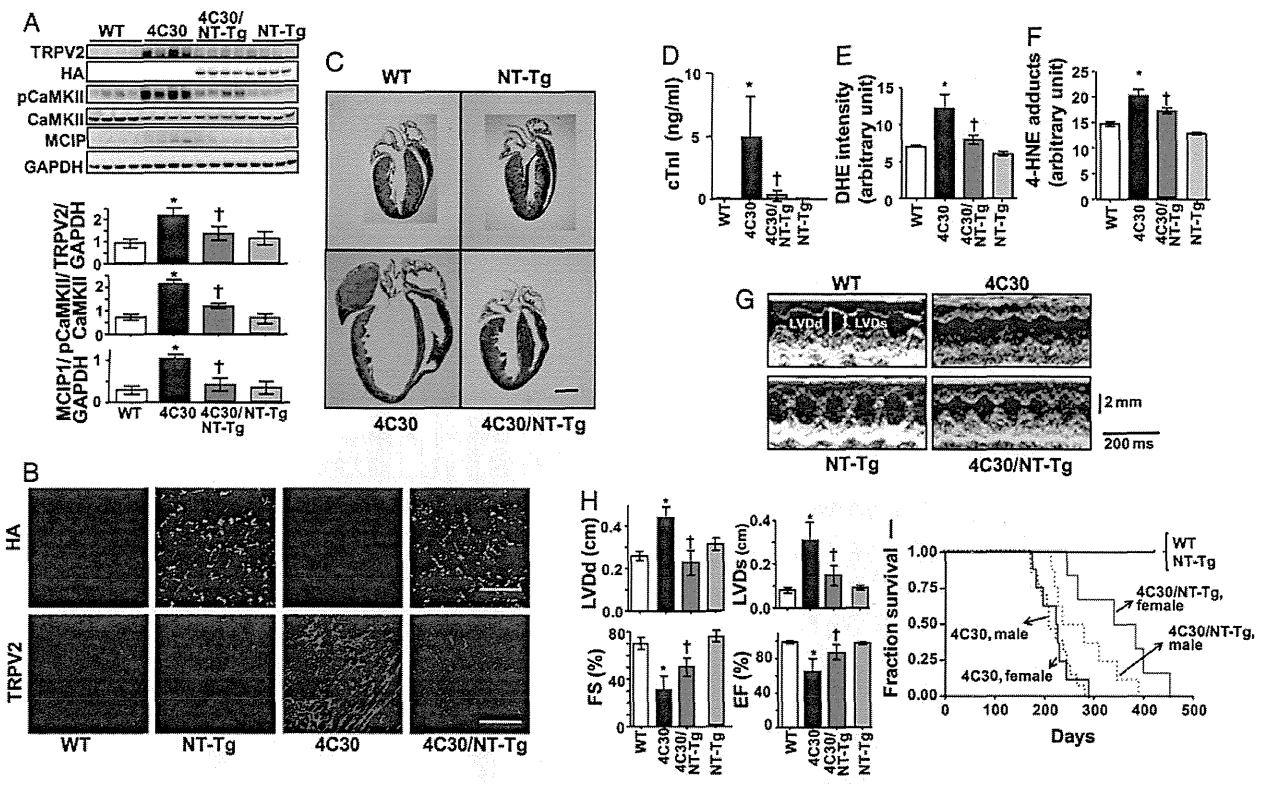

Figure 4 Over-expression of the NT domain blocks TRPV2 surface expression and ameliorates morphological and biochemical symptoms of cardiomyopathy in 4C30 mice. (*A*) Representative immunoblot of heart homogenates with the indicated antibodies (upper panel). Data represent values from four independent experiments ($n = 3$–4/group) $^{*}P < 0.05$ vs. WT mice, $^{\dagger}P < 0.05$ vs. 4C30 mice. (*B*) Representative immunohistochemical data from longitudinal cardiac sections from each group of mice. Scale bar: 100 μm. (*C*) Cardiac sections from 150-day-old mice stained with Masson's trichrome. Scale bar: 5 mm. (*D*) Level of cTnI in serum ($n = 10$ mice/group). (*E*) Superoxides produced in the hearts were analysed by staining the ventricular tissues with DHE. (*F*) Immunostaining data of the hearts with 4-HNE antibody were analysed ($n = 3$ mice/group) $^{*}P < 0.05$ vs. WT mice, $^{\dagger}P < 0.05$ vs. 4C30 mice. (*G*) Representative echocardiograms of each group of mice. (*H*) Echocardiographic analysis of cardiac function. (*I*) Kaplan–Meier survival analysis of each group of mice ($n = 25$–30 mice/group).

cardiac muscles and that the surface membrane expression of TRPV2 was decreased by NT domain over-expression. Echocardiography revealed that NT domain over-expression resulted in good amelioration of cardiac dysfunction, with improved FS and EF and reduced fibrosis (*Figure 6C–E*). These results demonstrated that NT domain-induced prevention of the sarcolemmal localization of TRPV2 can greatly ameliorate gene-defective DCM.

3.6 Tranilast prevents cardiomyopathy in J2N-k hamsters

We previously found that tranilast, which is known to be a non-selective cation channel blocker, effectively inhibits TRPV2.[22] Tranilast inhibited 2-APB-induced $[Ca^{2+}]_i$ increases with half-maximal inhibition at about 30 μM, in HEK293 cells expressing TRPV2 (Supplementary material online, *Figure S5*), but it has almost no effect on HEK293 cells expressing TRPV1, TRPV3, or TRPC1 (Supplementary material online, *Figure S5*). A recent study reported that tranilast inhibits TRPV2 ion channel activity.[23] Thus, tranilast is one of the better inhibitors presently available against TRPV2. We observed that tranilast reduced the amount of surface TRPV2 and abnormal Ca^{2+} mobilization by 2-APB in DCM cardiomyocytes (J2N-k, 4C30; unpublished observation). Oral administration of tranilast to J2N-k hamsters resulted in the effective removal of TRPV2 from the sarcolemma of J2N-k hearts (*Figure 6F*), similar to the effect of TRPV2 NT domain over-expression. Tranilast markedly reduced ventricular dilation and muscle fibrosis in J2N-k hearts (*Figure 6G*). Furthermore, it improved cardiac contraction, as evidenced by a decrease in echocardiographic parameters (LVDd and LVDs) to control levels (*Figure 6H*) and improved FS (*Figure 6H*).

4. Discussion

The present results suggest, for the first time, the pathological significance of TRPV2 in DCM development. First, TRPV2 was observed to be extensively localized to the ventricular sarcolemma in DCM patients as well as in animal models of heart failure (J2N-k, 4C30, and DOX-induced cardiomyopathic mice), whereas it localized to the intracellular compartments and intercalated discs in normal ventricles. Second, Tg or adenoviral NT domain over-expression significantly reduced the sarcolemmal accumulation of TRPV2 and simultaneously ameliorated cardiac dysfunction, preventing DCM progression and improving survival in the animal models. Third, the TRPV2 inhibitor tranilast effectively prevented DCM progression in J2N-k hamsters. Based on these findings, we

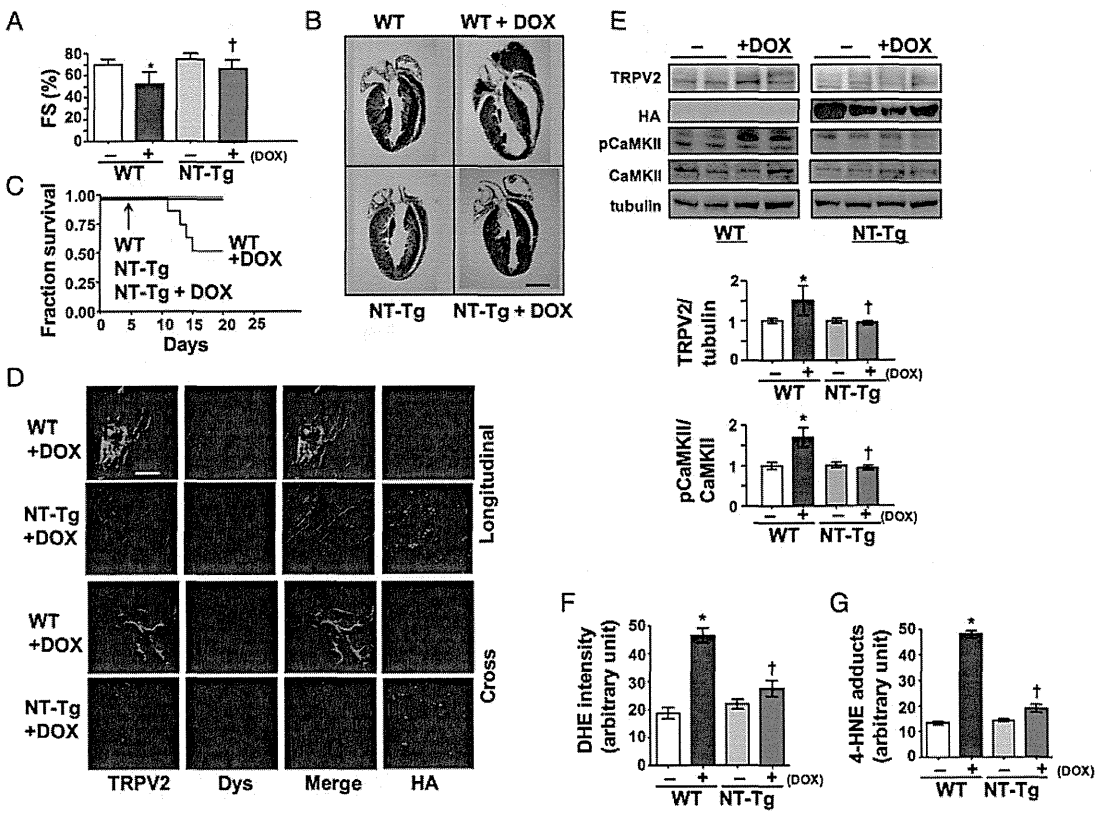

Figure 5 Over-expression of the NT domain ameliorates DOX-induced cardiomyopathy. (*A*) Echocardiographic analysis of cardiac function ($n = 6$ mice/group); $^*P < 0.05$ vs. without DOX, $^\dagger P < 0.05$ vs. WT with DOX. (*B*) Cardiac sections from 11-week-old DOX-treated or untreated WT or NT-Tg mice were stained with Masson's trichrome. Scale bar: 5 mm. (*C*) Kaplan–Meier survival analysis of each group of mice ($n = 15$ mice/group). (*D*) Immunohistochemical analysis of longitudinal (upper panel) and cross-sections (lower panel) of hearts from each group of mice. Scale bar: 100 μm. TRPV2, dystrophin (Dys) and HA antibodies were used. (*E*) Representative immunoblot data of heart homogenates from DOX-treated or untreated WT mice or NT-Tg with the indicated antibodies (left). TRPV2 expression levels are shown relative to tubulin expression and the extent of CaMKII phosphorylation is shown relative to total CaMKII levels (right). The data represent values from three independent experiments. (*F* and *G*) Levels of oxidative stress markers ($n = 4$ mice/group), $^*P < 0.05$ vs. without DOX, $^\dagger P < 0.05$ vs. WT with DOX.

hypothesize that the amelioration of DCM resulted from the inhibition of the Ca^{2+} influx through TRPV2; therefore, TRPV2 may be a potential upstream target against abnormal Ca^{2+} handling.

The DCM phenotype results from a broad variety of primary and secondary aetiologies. Despite the various underlying causes, there are many similarities in the final structural, functional, biochemical, and molecular phenotypes related to the long-lasting mechanical stress and neurohormonal activation observed in DCM.[24] CaMKII is an ideal nodal molecule for transducing Ca^{2+} signals into downstream events such as apoptosis and necrosis, leading to clinical phenotypes of congestive heart failure and sudden death.[25] In addition to CaMKII activation, ROS production is frequently observed in DCM hearts, with detrimental effects on cardiomyocytes.[26] We found that increased CaMKII phosphorylation and ROS production observed in DCM hearts were attenuated by over-expression of the NT domain of TRPV2 (*Figures 4* and *5*), suggesting that TRPV2 may be an upstream regulator of Ca^{2+} influx and ROS production as well as an important mediator of various stress signals, including those arising from genetic defects, mechanical stress, and cardiotoxic drugs, leading to Ca^{2+}-induced cell death. In addition, calcineurin is known to be an important Ca^{2+}-dependent signalling molecule leading to cardiac hypertrophy.[27] Certainly, cardiomyocyte-specific over-expression of calcineurin causes hypertrophy [28] and cardiomyopathy, but conflicting results are reported on the effects of calcineurin inhibition.[29] In our DCM models, calcineurin was slightly activated, as determined by the increase in the expression level of MCIP protein (*Figure 4*) as well as CaMKII activation and inhibition of TRPV2 suppressed both Ca^{2+}-signalling pathways (*Figure 4*). These findings suggest TRPV2 as a putative therapeutic target for the treatment of heart failure.

Here, we used 4C30 mice as a model for human idiopathic DCM. Unlike J2N-k hamsters, which gradually develop DCM, 4C30 mice are apparently asymptomatic up to 100 days but thereafter rapidly exhibit DCM symptoms and die within 200 days. Similar to that in 4C30 mice,[16] sialytransferase expression levels are altered in human DCM.[30] 4C30 mice also show DGC abnormalities (Supplementary material online, *Figure S4*), similar to those in DCM patients (*Figure 2A* and *B*). These characteristics indicate a pointed resemblance between 4C30 mice and human idiopathic DCM. Dystrophin degradation by the Ca^{2+}-dependent protease calpain was proposed as a pathway in

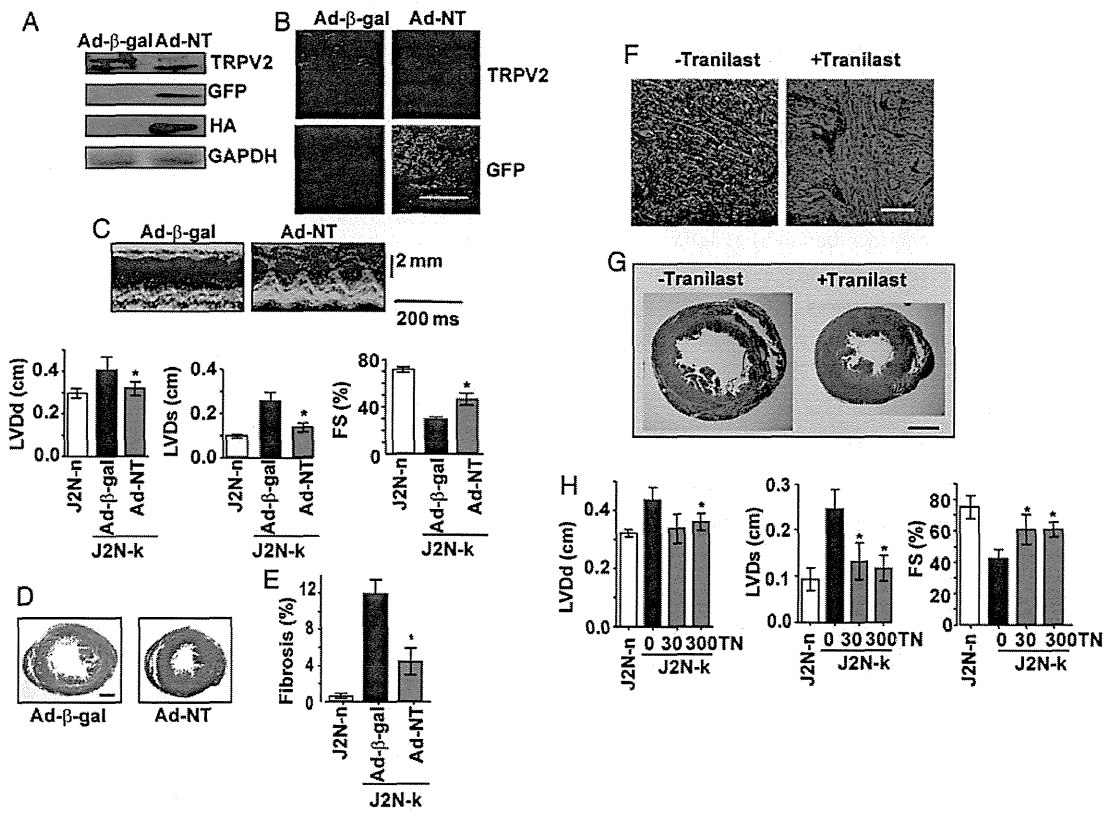

Figure 6 Two inhibitory tools against TRPV2 show comparative amelioration of cardiomyopathy in J2N-k. (*A*) Representative immunoblot and (*B*) immunohistochemical data of heart homogenates or sections from 11-week-old J2N-k infected with adenovirus carrying β-galactosidase (Ad-β-gal, control) or the NT domain (Ad-NT). Adenoviral infection was confirmed by staining with GFP. Scale bar: 100 μm. Similar results were obtained from three independent experiments. (*C*) Echocardiographic analysis of adenovirus-infected J2N-k. Representative echocardiograms (upper panels) and statistical evaluation (lower panels; $n = 6$ hearts/group); $^*P < 0.05$ vs. control. (*D*) Masson's trichrome staining of cardiac sections from adenovirus-infected J2N-k. (*E*) Fibrotic areas were analysed ($n = 6$ hearts/group). (*F*) J2N-k hamsters were administered none (−) or (+) tranilast (300 mg/kg per day) for 2 weeks, and the obtained tissues were immunostained with TRPV2 antibody. Tranilast prevented the sarcolemmal accumulation of TRPV2. Scale bar: 100 μm. (*G*) Heart sections from J2N-k hamsters were stained with Masson's trichrome. Tranilast ameliorated ventricular dilation and reduced fibrosis in these hamsters. Scale bar: 5 mm. (*H*) Effect of tranilast (TN) (0, 30, 300 mg/kg) on echocardiographic parameters in J2N-k ($n = 5$–8 hamsters/group); $^*P < 0.05$ vs. no treatment in J2N-k.

advanced heart failure with DCM symptoms.[31] Therefore, TRPV2 remodelling appears to be linked to sarcolemmal instability caused by DGC defects in various models of advanced heart failure. Thus, the 4C30 mouse appears to be a good animal model to study the connection between Ca^{2+} abnormality and DCM symptoms.

Plasma membrane TRPV2 translocation is known to be stimulated by receptor agonists[15,32] or mechanical stress.[15] Stimulation by growth factors or sympathetic transmitters could act as a signal inducing sarcolemmal TRPV2 translocation in DCM, because these stimulants are known to be released into the blood vessels of diseased hearts in response to mechanical load.[33] Considering that the TRPV2 inhibitory tools abrogated the surface expression of TRPV2 (*Figure 6*), Ca^{2+} influx via TRPV2 may also be important for sarcolemmal TRPV2 accumulation. Although further confirmatory studies are required, we suspect that NT domain over-expression inhibited membrane retention of TRPV2 by disrupting the interaction between TRPV2 and its putative binding partner, which regulates subcellular localization. Recently, a peptide mimetic of the CT domain of connexin 43 was used to disrupt the interaction between connexin 43 and the PDZ2 domain of zonula occludens-1 and reduce gap junction remodelling in injured hearts.[34]

Tranilast prevented ventricular dilation and fibrosis and ameliorated decreased FS by ~50% in J2N-k hamsters (*Figure 6*). These beneficial effects were comparable to those obtained from the adenoviral transfer of the NT domain (*Figure 6*). These treatments were performed in 9-week-old J2N-k hamsters that had already started displaying DCM symptoms. Therefore, our approach may be useful as a therapeutic intervention against the initial symptoms of DCM. Similar results using different strategies (chemical vs. protein) strongly suggest that TRPV2 activity contributes to DCM progression. Importantly, tranilast is immediately available for patients as an anti-inflammatory compound, since it reportedly has anti-inflammatory and immunomodulatory effects;[35] therefore, it may have clinical potential in DCM therapy. Recently, consistent with our data, tranilast has been reported to reduce both functional and structural abnormalities in diabetic cardiomyopathic rats[36] and prevent the progression from compensated hypertrophy to heart failure in pressure-overloaded mice.[37] The latter study suggested that tranilast reduced the heart-failure progression by acting as a mast-cell stabilizer. Since TRPV2 was reported to be involved in mast-cell degranulation,[38] TRPV2 may be also responsible for tranilast-induced amelioration of heart failure.

In conclusion, specific abrogation of TRPV2 activity by either NT domain over-expression or chemical inhibitor treatment led to considerable amelioration of cardiac pathology in the animal models. Our findings strongly suggest that the sarcolemmal TRPV2 accumulation plays a crucial role in Ca^{2+}-induced muscle degeneration in DCM and that TRPV2 is a good therapeutic target for advanced heart failure.

Supplementary material

Supplementary material is available at *Cardiovascular Research* online.

Acknowledgements

We thank Dr Hatsue Ueda (NCVC) for kindly providing us with information for human samples and Dr Yuji Arai (NCVC) for technical support in Tg production.

Conflict of interest: none declared.

Funding

This work was supported by a Grant-in-Aid for Priority Areas (grant number 18077015) to S.W.; Grants-in-Aid (grant numbers 19390080, 17659241 (to S.W.), 18590796, 20590874 (to Y.I.)); and a Grants-in-Aid (grant number 22659046) for Exploratory Research to S.W. from the Japanese Ministry of Education, Culture, Sports, Science and Technology; a grant for the Promotion of Fundamental Studies in Health Sciences of the National Institute of Biomedical Innovation; research grants for Cardiovascular Diseases (grant number 17A-1) to S.W. and Nervous and Mental Disorders (grant numbers 16B-2 and 19A-7) to Y.I. from the Japanese Ministry of Health, Labour and Welfare.

References

1. Hughes SE, McKenna WJ. New insights into the pathology of inherited cardiomyopathy. *Heart* 2005;**91**:257–264.
2. Fatkin D, Graham RM. Molecular mechanisms of inherited cardiomyopathies. *Physiol Rev* 2002;**82**:945–980.
3. Seidman JG, Seidman C. The genetic basis for cardiomyopathy: from mutation identification to mechanistic paradigms. *Cell* 2001;**104**:557–567.
4. Jefferies JL, Towbin JA. Dilated cardiomyopathy. *Lancet* 2010;**375**:752–762.
5. Campbell KP, Kahl SD. Association of dystrophin and an integral membrane glycoprotein. *Nature* 1989;**338**:259–262.
6. Nigro V, Okazaki Y, Belsito A, Piluso G, Matsuda Y, Politano L *et al.* Identification of the Syrian hamster cardiomyopathy gene. *Hum Mol Genet* 1997;**6**:601–607.
7. Jeong EM, Liu M, Sturdy M, Gao G, Varghese ST, Sovari AA *et al.* Metabolic stress, reactive oxygen species, and arrhythmia. *J Mol Cell Cardiol* 2012;**52**:454–463.
8. Toko H, Takahashi H, Kayama Y, Oka T, Minamino T, Okada S *et al.* Ca^{2+}/calmodulin-dependent kinase IIdelta causes heart failure by accumulation of p53 in dilated cardiomyopathy. *Circulation* 2010;**122**:891–899.
9. Beuckelmann DJ, Nabauer M, Erdmann E. Intracellular calcium handling in isolated ventricular myocytes from patients with terminal heart failure. *Circulation* 1992;**85**:1046–1055.
10. Lindner M, Brandt MC, Sauer H, Hescheler J, Bohle T, Beuckelmann DJ. Calcium sparks in human ventricular cardiomyocytes from patients with terminal heart failure. *Cell Calcium* 2002;**31**:175–182.
11. Louch WE, Bito V, Heinzel FR, Macianskiene R, Vanhaecke J, Flameng W *et al.* Reduced synchrony of Ca^{2+} release with loss of T-tubules-a comparison to Ca^{2+} release in human failing cardiomyocytes. *Cardiovascular Research* 2004;**62**:63–73.
12. Eder P, Molkentin JD. TRPC channels as effectors of cardiac hypertrophy. *Circ Res* 2011;**108**:265–272.
13. Nilius B, Owsianik G, Voets T, Peters JA. Transient receptor potential cation channels in disease. *Physiol Rev* 2007;**87**:165–217.
14. Watanabe H, Murakami M, Ohba T, Takahashi Y, Ito H. TRP channel and cardiovascular disease. *Pharmacol Therap* 2008;**118**:337–351.
15. Iwata Y, Katanosaka Y, Arai Y, Komamura K, Miyatake K, Shigekawa M. A novel mechanism of myocyte degeneration involving the Ca^{2+}-permeable growth factor-regulated channel. *J Cell Biol* 2003;**161**:957–967.
16. Suzuki O, Kanai T, Nishikawa T, Yamamoto Y, Noguchi A, Takimoto K *et al.* Adult onset cardiac dilatation in a transgenic mouse line with Galβ1,3GalNAc α2,3-sialyltransferase II (ST3Gal-II) transgenes: a new model for dilated cardiomyopathy. *Proc Japan Acad, SerB* 2011;**87**:550–562.
17. Iwata Y, Katanosaka Y, Arai Y, Shigekawa M, Wakabayashi S. Dominant-negative inhibition of Ca2+ influx via TRPV2 ameliorates muscular dystrophy in animal models. *Hum Mol Genet* 2009;**18**:824–834.
18. Iwata Y, Pan Y, Hanada H, Yoshida T, Shigekawa M. Dystrophin-glycoprotein complex purified from hamster cardiac muscle. Comparison of the complexes from cardiac and skeletal muscles of hamster and rabbit. *J Mol Cell Cardiol* 1996;**28**:2501–2509.
19. Nakamura TY, Iwata Y, Arai Y, Komamura K, Wakabayashi S. Activation of Na^+/H^+ exchanger 1 is sufficient to generate Ca^{2+} signals that induce cardiac hypertrophy and heart failure. *Circ Res* 2008;**103**:891–899.
20. Hu HZ, Gu Q, Wang C, Colton CK, Tang J, Kinoshita-Kawada M *et al.* 2-aminoethoxydiphenyl borate is a common activator of TRPV1, TRPV2, and TRPV3. *J Biol Chem* 2004;**279**:35741–35748.
21. Lievremont JP, Bird GS, Putney JW Jr. Mechanism of inhibition of TRPC cation channels by 2-aminoethoxydiphenylborane. *Mol Pharmacol* 2005;**68**:758–762.
22. Iwata Y, Katanosaka Y, Shijun Z, Kobayashi Y, Hanada H, Shigekawa M *et al.* Protective effects of Ca^{2+} handling drugs against abnormal Ca^{2+} homeostasis and cell damage in myopathic skeletal muscle cells. *Biochem Pharmacol* 2005;**70**:740–751.
23. Mihara H, Boudaka A, Shibasaki K, Yamanaka A, Sugiyama T, Tominaga M. Involvement of TRPV2 activation in intestinal movement through nitric oxide production in mice. *J Neurosci* 2010;**30**:16536–16544.
24. Houser SR, Margulies KB, Murphy AM, Spinale FG, Francis GS, Prabhu SD *et al.* Animal models of heart failure: a scientific statement from the American Heart Association. *Circ Res* 2012;**111**:131–150.

25. Anderson ME. CaMKII and a failing strategy for growth in heart. *J Clin Invest* 2009;**119**: 1082–1085.
26. Giordano FJ. Oxygen, oxidative stress, hypoxia, and heart failure. *J Clin Invest* 2005;**115**: 500–508.
27. Wilkins BJ, Dai YS, Bueno OF, Parsons SA, Xu J, Plank DM *et al.* Calcineurin/NFAT coupling participates in pathological, but not physiological, cardiac hypertrophy. *Circ Res* 2004; **94**:110–118.
28. Molkentin JD, Lu JR, Antos CL, Markham B, Richardson J, Robbins J *et al.* A calcineurin-dependent transcriptional pathway for cardiac hypertrophy. *Cell* 1998;**93**:215–228.
29. Wilkins BJ, Molkentin JD. Calcium-calcineurin signaling in the regulation of cardiac hypertrophy. *Biochem Biophys Res Commun* 2004;**322**:1178–1191.
30. Hwang JJ, Allen PD, Tseng GC, Lam CW, Fananapazir L, Dzau VJ *et al.* Microarray gene expression profiles in dilated and hypertrophic cardiomyopathic end-stage heart failure. *Physiol Genom* 2002;**10**:31–44.
31. Toyo-Oka T, Kawada T, Nakata J, Xie H, Urabe M, Masui F *et al.* Translocation and cleavage of myocardial dystrophin as a common pathway to advanced heart failure: a scheme for the progression of cardiac dysfunction. *Proc Natl Acad Sci USA* 2004;**101**:7381–7385.
32. Kanzaki M, Zhang YQ, Mashima H, Li L, Shibata H, Kojima I. Translocation of a calcium-permeable cation channel induced by insulin-like growth factor-I. *Nat Cell Biol* 1999;**1**: 165–170.
33. Ruwhof C, van der Laarse A. Mechanical stress-induced cardiac hypertrophy: mechanisms and signal transduction pathways. *Cardiovasc Res* 2000;**47**:23–37.
34. O'Quinn MP, Palatinus JA, Harris BS, Hewett KW, Gourdie RG. A peptide mimetic of the connexin43 carboxyl terminus reduces gap junction remodeling and induced arrhythmia following ventricular injury. *Circ Res* 2011;**108**:704–715.
35. Pae HO, Jeong SO, Koo BS, Ha HY, Lee KM, Chung HT. Tranilast, an orally active anti-allergic drug, up-regulates the anti-inflammatory heme oxygenase-1 expression but down-regulates the pro-inflammatory cyclooxygenase-2 and inducible nitric oxide synthase expression in RAW264.7 macrophages. *Biochem Biophys Res Commun* 2008;**371**: 361–365.
36. Kelly DJ, Zhang Y, Connelly K, Cox AJ, Martin J, Krum H *et al.* Tranilast attenuates diastolic dysfunction and structural injury in experimental diabetic cardiomyopathy. *Am J Physiol Heart Circ Physiol* 2007;**293**:H2860–H2869.
37. Hara M, Ono K, Hwang MW, Iwasaki A, Okada M, Nakatani K *et al.* Evidence for a role of mast cells in the evolution to congestive heart failure. *J Exp Med* 2002;**195**: 375–381.
38. Zhang D, Spielmann A, Wang L, Ding G, Huang F, Gu Q *et al.* Mast-cell degranulation induced by physical stimuli involves the activation of transient-receptor-potential channel TRPV2. *Physiol Res* 2012;**61**:113–124.

Opposing Immunomodulatory Roles of Prostaglandin D_2 during the Progression of Skin Inflammation

Hana Sarashina,* Yoshiki Tsubosaka,† Keisuke Omori,* Kosuke Aritake,‡ Takayuki Nakagawa,§ Masatoshi Hori,* Hiroyuki Hirai,¶ Masataka Nakamura,‖ Shuh Narumiya,# Yoshihiro Urade,‡ Hiroshi Ozaki,* and Takahisa Murata†

The effects of PGD_2 are extremely context dependent. It can have pro- or anti-inflammatory effects in clinically important pathological conditions. A greater mechanistic insight into the determinants of PGD_2 activity during inflammation is thus required. In this study, we investigated the role of PGD_2 in croton oil–induced dermatitis using transgenic (TG) mice overexpressing hematopoietic PGD synthase. Administration of croton oil caused tissue swelling and vascular leakage in the mouse ear. Compared with wild-type animals, TG mice produced more PGD_2 and showed decreased inflammation in the early phase, but more severe manifestations during the late phase. Data obtained from bone marrow transplantation between wild-type and TG mice indicated that PGD_2 produced by tissue resident cells in the TG mice attenuated early-phase inflammation, whereas PGD_2 produced from hematopoietic lineage cells exacerbated late-phase inflammation. There are two distinct PGD_2 receptors: D-prostanoid receptor (DP) and chemoattractant receptor–homologous molecule expressed on Th2 cells (CRTH2). In TG mice, treatment with a DP antagonist exacerbated inflammation in the early phase, whereas treatment with a CRTH2 antagonist attenuated inflammation during the late phase. In vitro experiments showed that DP agonism enhanced vascular endothelial barrier formation, whereas CRTH2 agonism stimulated neutrophil migration. Collectively, these results show that when hematopoietic PGD synthase is overexpressed, tissue resident cell–derived PGD_2 suppresses skin inflammation via DP in the early phase, but hematopoietic lineage cell–derived PGD_2 stimulates CRTH2 and promotes inflammation during the late phase. DP-mediated vascular barrier enhancement or CRTH2-mediated neutrophil activation may be responsible for these effects. Thus, PGD_2 represents opposite roles in inflammation, depending on the disease phase in vivo. *The Journal of Immunology*, **2014, 192: 459–465.**

Prostaglandins are metabolites of arachidonic acid generated by cyclooxygenase (COX) that are synthesized and released upon encountering injurious stimuli. COX-mediated PG synthesis is generally categorized as a proinflammatory event. For instance, a major PG, PGE_2, triggers common inflammatory symptoms, including swelling, pain, and fever (1, 2). Another prostanoid, TXA_2, promotes platelet aggregation and vascular contraction (3). Clinically, inhibition of COX-mediated PG synthesis has been applied to treat several types of inflammatory diseases, including arthritis (4) and colorectal cancer (5).

PGD_2 is reported to promote sleep and to mediate inflammatory responses. PGD synthase is of two types: lipocalin-type PGD synthase and hematopoietic PGD synthase (H-PGDS). Lipocalin-type PGD synthase is expressed mainly in the arachnoid and choroid membrane, and is implicated in sleep (6) and pain promotion (7). In contrast, H-PGDS is expressed mainly in immune cells, such as mast cells and Th2 lymphocytes, and contributes to various inflammatory responses in peripheral tissues (8). PGD_2 exerts its effects via two types of receptors: D-prostanoid receptor (DP) and chemoattractant receptor–homologous molecule expressed on Th2 cells (CRTH2). The half-life of PGD_2 in blood is short (0.9 min) (9). Several in vitro and in vivo studies have shown that PGD_2 is quickly degraded to several products through enzymatic and/or nonenzymatic pathways (10, 11), and that these products also stimulate PGD_2-dependent pathways. Whereas PGD_2 and its degradation product, PGJ_2, can bind DP and CRTH2 equally, many of the other products, such as $9\alpha,11\beta$-PGF_2, 13,14-dihydro-15-keto-PGD_2 (DK-PGD_2), and 15-deoxy-$\Delta^{12,14}$-PGD_2 (15d-PGD2), possess higher binding affinity for CRTH2 (12–14). J-ring PGs also exhibit bioactivity, as they are ligands for the peroxisome proliferator–activated receptor-γ (15–17). Although the pathophysiological implications of each PGD_2 metabolite in vivo remain elusive, various activities have been ascribed to these degradation products.

Reports have proved contradictory regarding whether PGD_2 is pro- or anti-inflammatory. For instance, administration of PGD_2 or a DP agonist has anti-inflammatory effects in rat bowel inflammation (18)

*Department of Veterinary Pharmacology, Graduate School of Agriculture and Life Sciences, The University of Tokyo, Tokyo 113-8657, Japan; †Department of Animal Radiology, Graduate School of Agriculture and Life Sciences, The University of Tokyo, Tokyo 113-8657, Japan; ‡Department of Molecular Behavioral Biology, Osaka Bioscience Institute, Osaka 565-0874, Japan; §Department of Veterinary Surgery, Graduate School of Agriculture and Life Sciences, The University of Tokyo, Tokyo 113-8657, Japan; ¶Advanced Medicine and Development, BML, Inc., Saitama 350-1101, Japan; ‖Human Gene Sciences Center, Tokyo Medical and Dental University, Tokyo 113-8150, Japan; and #Department of Pharmacology, Faculty of Medicine, Kyoto University, Kyoto 606-8315, Japan

Received for publication August 7, 2013. Accepted for publication November 1, 2013.

This work was supported by the Program for Promotion of Basic and Applied Researches for Innovations in Bio-oriented Industry (Grant 12100979); the Ministry of Education, Culture, Sports, Science and Technology and the Japan Society for the Promotion of Science (Grants 22688024 and 25252049); the Mochida Memorial Foundation; and the Towa Foundation (to T.M.).

Address correspondence and reprint requests to Prof. Takahisa Murata, Department of Animal Radiology, Graduate School of Agriculture and Life Sciences, University of Tokyo, 1-1-1 Yayoi, Bunkyo-ku, Tokyo 113-8657, Japan. E-mail address: amurata@mail.ecc.u-tokyo.ac.jp

The online version of this article contains supplemental material.

Abbreviations used in this article: BAEC, bovine aortic endothelial cell; BM, bone marrow; BMT, bone marrow transplantation; COX, cyclooxygenase; CRTH2, chemoattractant receptor–homologous molecule expressed on Th2 cell; $CRTH2^{-/-}$, CRTH2 deficient; DK-PGD_2, 13,14-dihydro-15-keto-PGD_2; DP, D-prostanoid receptor; $DP^{-/-}$, DP deficient; H-PGDS, hematopoietic PGD synthase; TER, transendothelial electric resistance; TG, transgenic; VEGF, vascular endothelial growth factor; WT, wild-type.

www.jimmunol.org/cgi/doi/10.4049/jimmunol.1302080

and mouse atopic dermatitis (19). DP receptor agonism inhibited eosinophil migration (20) and dendritic cell activation (21) in a mouse model of asthma. Our group also proved that PGD_2 suppressed mouse acute lung inflammation and tumor growth by inhibiting vascular permeability and subsequent angiogenesis via DP stimulation (22, 23). According to these observations, the PGD_2-DP axis is likely to exert anti-inflammatory effects. In contrast, several other groups showed that PGD_2 signaling mediates proinflammatory responses. For example, administration of an H-PGDS inhibitor improved mouse airway inflammation (24). Furthermore, treatment with a CRTH2 agonist aggravated atopic dermatitis and asthma in mice, whereas intratracheal administration of PGD_2 promoted eosinophil migration in rats (25, 26). Thus, PGD_2 is likely to regulate inflammation differently, depending on the disease type.

The overall outcome of an inflammatory response is determined by multiple factors, including the type of mediator-producing cell/effector cell, the precise effector cell function, the amount of inflammatory signal produced, and the identity of the receptor receiving the stimulus. Furthermore, these factors vary according to the site and phase of inflammation. Because PGD_2 and its metabolites exert various actions through several signal pathways, detailed studies investigating where and how PGD_2 is produced, and its effects in discrete phases of discrete diseases, are indispensable for the design of future therapies.

In the current study, we compared inflammatory reactions in the skin between transgenic (TG) mice overexpressing H-PGDS and wild-type (WT) mice to evaluate the contribution of PGD_2 at each stage of disease progression. We demonstrate that PGD_2-DP signaling originating in tissue resident cells alleviates vascular permeability in the early phase of croton oil–induced dermatitis, and that PGD_2-CRTH2 signaling in infiltrating hematopoietic cells promotes inflammation during the late phase of dermatitis.

Materials and Methods

Reagents

Croton oil, vascular endothelial growth factor (VEGF), and Evans blue were from Sigma-Aldrich; Triton X-100, paraformaldehyde, formamide, and methyl acetate were from Wako Pure Chemical; PGD_2, BW 245C, BW A868C, CAY10471, AL 8810, SQ29548, 15-deoxy-$\Delta^{12,14}$-PGD_2, 9α,11β-PGF_2, DK-PGD_2, anti–H-PGDS Ab, and anti–COX-2 Ab were from Cayman Chemical; anti-CD45 Ab was from Millipore; and penicillin-streptomycin was from Life Technologies.

Mouse dermatitis model

All animal experiments were performed in accordance with the guidelines of the University of Tokyo. TG mice with FVB background expressing human H-PGDS under the regulatory control of the chicken β-actin promoter were generated as previously described (27). Among the three lines of TG mice (S41, S55, and S66), S55 was used, as they exhibited the most abundant mRNA expression and enzymatic activity of human H-PGDS. DP deficient ($DP^{-/-}$) and CRTH2 deficient ($CRTH2^{-/-}$) mice with C57BL/6 background were generated and bred as described previously (28, 29). In some experiments, bone marrow transplantation (BMT) was performed as previously described (22). Recipient mice (4–5 wk old) were irradiated with 4.5 Gy, twice with 12-h intervals. Bone marrow (BM) cells (2×10^5) were collected from femurs of donor mice (8–9 wk old) and injected through the tail vein of the recipient. Mice were used for each experiment 8 wk after BMT. Mice were anesthetized with isoflurane. Croton oil (2.5%, 2 h or 6 h) was administered to the surface of the right ear of mice. VEGF (30 ng per head, 35 min), 9α,11β-PGF_2 (10 ng per head each, 40 min), or DK-PGD_2 (10 ng per head each, 40 min) was injected s.c. into the right ear. Vehicle was administered to the left ear as an internal control.

Modified Miles assay

After a certain period from the time of administration of each reagent to the ears, mice were i.v. injected with Evans blue (30 mg/kg for FVB TG mice or 50 mg/kg for C57BL/6 gene-deficient mice). At 30 min after the circulation, the ears were dissected and dried overnight at 55°C. After the ears were weighed, Evans blue was extracted by incubation in formamide at 55°C for 24 h. Dye content was measured by reading at 610 nm in a spectrophotometer (Wallac 1420, PerkinElmer) and normalized to ear dry weight.

Measurement of PGs

Contents of PGD_2, PGE_2, and TXA_2 in ears were measured as previously described (30). Briefly, excised ears were quickly frozen into liquid nitrogen and homogenized in ethanol containing 0.02% HCl, and the samples were separated by HPLC. An API3200 triple-quadruple tandem mass spectrometer (Applied Biosystems) was used.

Immunostaining

Ear tissues were fixed in 4% paraformaldehyde for 2 d and embedded in paraffin. Sections of 4-μm thickness were stained with H&E. For immunostaining, 5-μm-thick frozen sections were used. After permeabilization/blocking with 0.1% Triton X-100 and 5% normal goat serum for 30 min, sections were labeled with anti–H-PGDS Ab (1:400), anti–COX-2 Ab (1:250), or anti-CD45 Ab (1:400) overnight at 4°C. Then, the sections were labeled with secondary Ab and DAPI. The images were captured using an Eclipse E800 fluorescence microscope (Nikon), and the number of $CD45^+$ cells was counted in three randomly chosen fields in each slide.

Measurement of transendothelial electric resistance

Bovine thoracic aortas were purchased from a slaughterhouse. Bovine aortic endothelial cells (BAECs) were isolated and cultured in DMEM containing 10% FBS. BAECs (2.5×10^4) were seeded into each well of the microelectronic sensor, and then transendothelial electric resistance (TER) was measured by xCELLigence real time cell analyzer DP system (Roche). Confluent monolayers of BAECs were serum starved for 10 h before the experiment. TER was measured every 30 s and then normalized to the initial value.

Isolation of neutrophil and chemotaxis assay

Marrow cavities of the tibias and femurs of 8-wk-old mice were flushed with DMEM. Neutrophils were isolated by centrifugation over discontinuous Percoll gradients. For the chemotaxis assay, a modified Boyden chamber

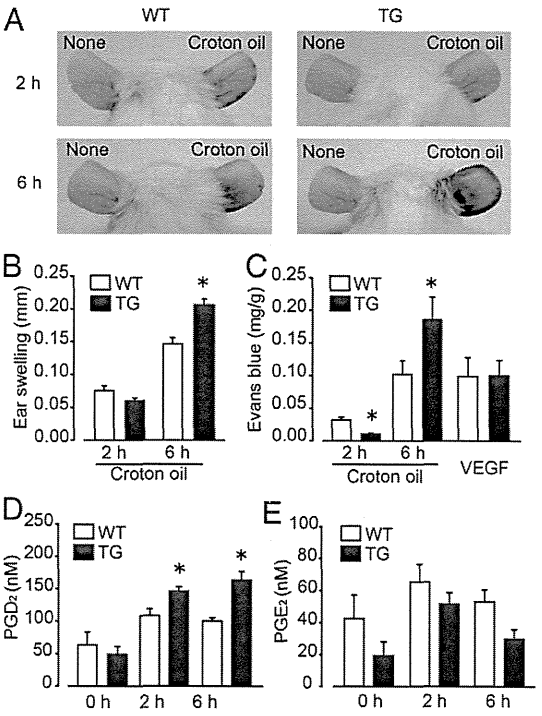

FIGURE 1. Croton oil–induced skin inflammation in H-PGDS–overexpressing mice. Croton oil (2.5%, 2 h or 6 h) or VEGF (30 ng, 35 min) was administered to mouse ears. Evans blue dye (30 mg/kg) was injected and circulated for 30 min. (**A**) Representative photographs show croton oil–induced inflammation. Skin thickness (**B**) or dye extravasation (**C**) of the inflamed ears was quantified (n = 5–8 each, $*p < 0.05$ compared with WT). The concentration of PGD_2 (**D**) or PGE_2 (**E**) in inflamed ears was determined by a mass spectrometer (n = 5, $*p < 0.05$ compared with WT).

with 8-μm pores (BD Falcon) was used. Stimulants were added to the bottom chamber, and inhibitors were added to both the upper and the bottom chambers. Isolated neutrophils (2×10^5 cells) were applied to the upper chambers. After 2 h, cells on the membrane were fixed and stained with Giemsa solution. The number of cells from five randomly chosen fields (×200) on the lower side of the membrane was counted.

Data representation and statistical analysis

The results are expressed as mean ± SEM. Statistical evaluations of the data were performed using an unpaired Student *t* test for comparisons between two groups and by one-way ANOVA followed by a Dunnett test or Tukey test for comparison between more than two groups. A $p < 0.05$ was taken as significant.

Results

Inflammatory responses in the presence of H-PGDS overexpression

In WT mice, administration of 2.5% croton oil caused ear swelling (Fig. 1B) and increased dye extravasation, an index of vascular permeability (typical pictures are shown in Fig. 1A, and dye leakages are quantified in Fig. 1C). These responses peaked 6 h after the stimulation and settled in 36 h (ear swelling, 6 h, 0.146 ± 0.013 mm; 36 h, 0.012 ± 0.005 mm, $n = 5$ each).

Pretreatment with a pan-COX inhibitor, indomethacin, inhibited these responses (Supplemental Fig. 1), suggesting the contributions of PG production to the inflammation. TG mice showed reduced severity of ear swelling and less vascular leakage at the early phase (2 h after the stimulation), but showed more severe inflammation than WT mice at the late phase (6 h post treatment). WT and TG mice responded similarly to treatment with VEGF, which directly stimulates vascular leakage without activation of the arachidonate cascade (Fig. 1C, *right bars*).

Administration of 2.5% croton oil induced PGD_2 production in both WT and TG mice (Fig. 1D). PGD_2 production in TGs, compared with that in WT mice, was significantly higher during the experiments. The concentration of another prostanoid, PGE_2, did not differ between the lines (Fig. 1E).

Infiltrated leukocytes expressed H-PGDS

As shown by the H&E staining (Fig. 2A, *upper panels*), no morphological difference was observed between WT and TG mice prior to stimulation (0 h). There was a time-dependent ear swelling and infiltration of inflammatory cells upon croton oil administration. Most of the infiltrating cells were neutrophils with segmented nuclei (Fig. 2A, *middle and lower panels*; see insets). Regarding the ear-swelling data shown in Fig. 1B, TG ears were slightly thinner at the early phase of inflammation, whereas they were much thicker than WT ears at the late phase. Neutrophil infiltration was also accelerated in TG mice at the late phase (Fig. 2A, inset panels).

We next performed immunostaining to define which type of cell expresses H-PGDS in inflamed ears. As shown in Fig. 2B (*upper left panels*), H-PGDS was not detected in nontreated WT ears. In croton oil–treated WT ears, $CD45^+$ leukocytes expressed H-PGDS (Fig. 2B, *middle and lower left panels*). TG ears broadly expressed H-PGDS regardless of oil stimulation (Fig. 2B, *left panels*). These observations are consistent with the fact that human H-PGDS is constitutively expressed in the TG mice from a chicken β-actin promoter. Of interest, oil stimulation increased H-PGDS expression even in TG mice, and in particular in the $CD45^+$ cells. This finding may be due to the elevation of endogenous mouse H-PGDS expression in response to stimulation.

Expression of an inducible type of COX, COX-2, is required to produce PGD_2 in the context of inflammation. As shown in Sup-

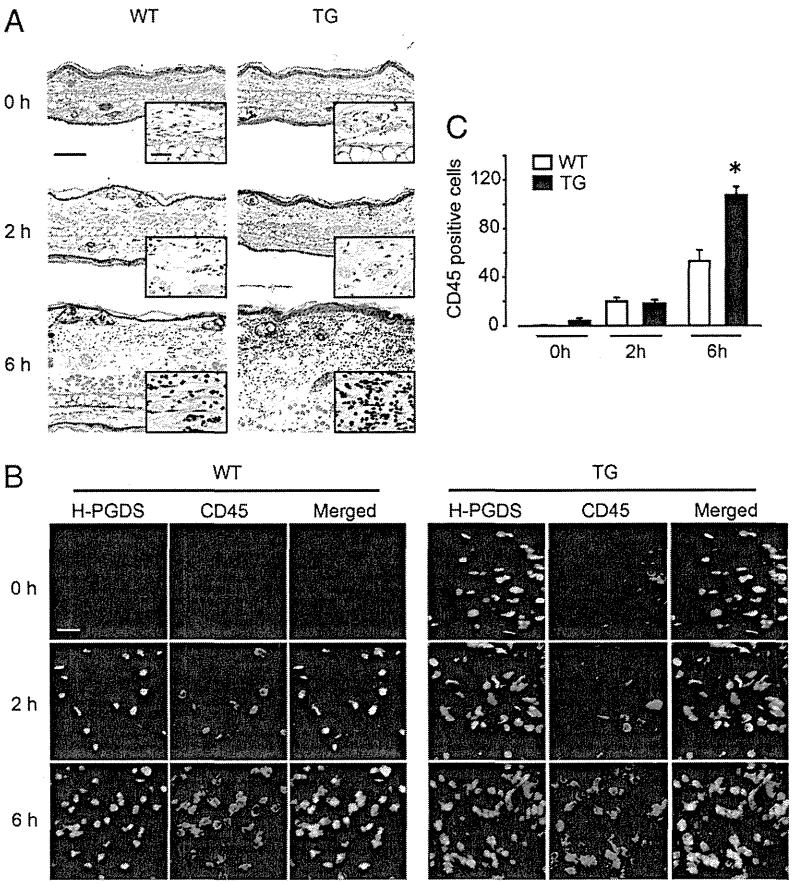

FIGURE 2. Infiltrating leukocytes expressed H-PGDS in inflamed ears. (**A**) Representative images of H&E stainingare shown. (**B**) Excised ears from WT or TG mice were subjected to immunostaining for H-PGDS (green) and CD45 (red), and then stained with DAPI (blue) for nuclear labeling ($n = 4$ each). The pictures were randomly taken from three fields, each at a magnification of ×200 from four dependent sections. Scale bar, 20 μm. (**C**) The number of $CD45^+$ cells was counted ($n = 4$, $^*p < 0.05$ compared with WT).

plemental Fig. 2A and 2B, $CD31^+$ vascular endothelial cells constitutively express COX-2 in both lines of mice. Infiltrating $CD45^+$ leukocytes (most likely neutrophils) also express COX-2 after stimulation. We thus inferred that these two cell types are the major sources of PGD_2 in this model.

In agreement with the observations from H&E staining, a significant difference was noted in the number of infiltrating leukocytes between the lines during the early phase of inflammation. In contrast, many more leukocytes infiltrated TG ears than WT ears at the late phase (Fig. 2C).

Functional contribution of hematopoietic lineage–derived PGD_2 in dermatitis

We explored the contribution of hematopoietic cell (BM-derived immune cells)– or nonhematopoietic cell (tissue resident cells)–derived PGD_2 in dermatitis using BMT. Irradiated WT recipients with WT BM (WT + WT^{BM}) exhibited tissue swelling comparable to that in nontreated WT (Supplemental Fig. 3) in response to oil treatment. The BMT procedures (i.e., radiation and BM injection) did not affect the inflammatory responses. At the early phase of inflammation (2 h), no difference was detected in ear swelling between the lines (Fig. 3A), whereas TG transplanted with WT or TG BM (TG + WT^{BM} and TG + TG^{BM}) exhibited blunted vascular leakage compared with WT with WT or TG BM (WT + WT^{BM} and WT + TG^{BM}) (Fig. 3B). These results suggest that PGD_2 secreted from the tissue resident cells inhibits the inflammation in TG mice during the early phase of dermatitis.

At the late phase, regardless of recipient genotype, mice transplanted with TG BM (WT + TG^{BM}, TG + TG^{BM}) showed more severe swelling (Fig. 3C) and vascular leakage (Fig. 3D) in comparison with the mice with WT BM (WT + WT^{BM}, TG + WT^{BM}). This finding indicates that PGD_2 from infiltrating hematopoietic cells (most presumably neutrophils) promotes inflammatory responses in the TG during this phase.

The role of PGD_2-DP signaling in the early phase of inflammation

We attempted to clarify how PGD_2 modulated inflammatory responses during early-phase dermatitis. Administration of an H-PGDS inhibitor, HQL-79 (50 mg/kg, i.p.), significantly enhanced tissue swelling (Fig. 4A) and vascular permeability (Fig. 4B) in both lines of mice. Upon H-PGDS inhibition, the degrees of ear swelling and dye extravasation were similar in WT and TG mice. As with H-PGDS inhibition, DP antagonism by BW A868C (1 mg/kg, i.p.) also promoted inflammatory responses in both WT and TG mice to the same degree (Fig. 4C, 4D).

Thus, the DP-mediated signal most likely contributed to the immunosuppressive reaction of PGD_2 in early-phase inflammation. In support of this idea, $DP^{-/-}$ mice were more responsive to croton oil stimulation than were WT mice, whereas $CRTH2^{-/-}$ mice exhibited responses comparable to those of WT mice. Additive treatment with PGD_2 (1 mg/kg, i.p.) inhibited the oil-induced vascular leakage in WT and $CRTH2^{-/-}$ mice, but not $DP^{-/-}$ mice (Fig. 4E). Furthermore, administration of a DP agonist, BW 245C (1 mg/kg, i.p.), strongly inhibited vascular leakage in WT ears (Fig. 4F).

The role of PGD_2-CRTH2 signaling in late-phase inflammation

We next assessed the contribution of PGD_2 to late-phase dermatitis. As shown in Fig. 5A and 5B (ear swelling and dye leakage, respectively), inhibition of H-PGDS by HQL-79 (50 mg/kg, i.p.) tended to increase the scores in WT mice, whereas it attenuated them in TG mice. As shown in Fig. 5C and 5D (both data are shown

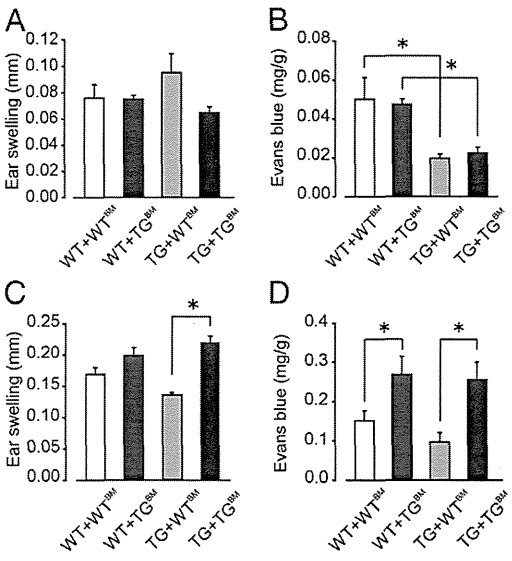

FIGURE 3. Contribution of hematopoietic lineage–derived PGD_2 in dermatitis. Ear swelling (thickness) and dye extravasation in each BMT mouse were assessed 2 h (**A** and **B**) or 6 h (**C** and **D**) after croton oil treatment (n = 5 or 6 each, $^*p < 0.05$).

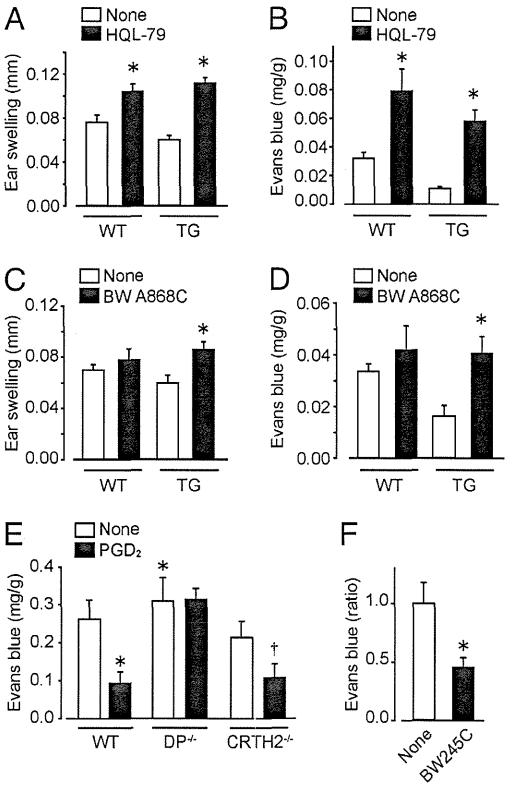

FIGURE 4. DP signaling alleviated early-phase inflammation. Effects of an H-PGDS inhibitor, HQL-79 (50 mg/kg, i.p., 3 h before the stimulation), or a DP antagonist, BW A868C (1 mg/kg, i.p., 2 h before the stimulation), on the ear swelling (**A** and **C**) and tissue dye extravasation (**B** and **D**) were assessed. Dye extravasation during early-phase inflammation were assessed in $DP^{-/-}$ or $CRTH2^{-/-}$ mice with C57BL/6 background (**E**). PGD_2 (1 mg/kg, i.p.) was administered 10 min before the stimulation. Effect of a DP agonist, BW 245C (1 mg/kg, i.p., 10 min before dye injection), on dye efflux during early-phase inflammation was assessed (**F**). The data are indicated as a ratio to nontreated ears (only with croton oil administration) (n = 4–6, $^*p < 0.05$ and $^\dagger p < 0.05$, compared with nontreated WT ears or $CRTH2^{-/-}$ ears).

as a ratio to nontreated), DP antagonism (BW A868C, 1 mg/kg i.p.) promoted, and CRTH2 antagonism (CAY10471, 1 mg/kg, i.p.) tended to attenuate, the oil-induced inflammation in both lines of mice. The DP-mediated anti-inflammatory reaction was dominant in WT mice, whereas the CRTH2-mediated proinflammatory signal appeared to counteract DP-mediated responses in TG mice.

We could obtain consistent observations using gene-deficient mice. As shown in Fig. 5E, WT and CRTH2$^{-/-}$ mice represented comparable vascular leakage responding to sole oil treatment (6 h). DP deficiency significantly increased vascular leakage even in late-phase dermatitis. Additional treatment with PGD_2 increased vascular permeability in WT and increased slightly, but not significantly, in DP$^{-/-}$ mice. In contrast, PGD_2 treatment significantly decreased vascular permeability in CRTH2$^{-/-}$ mice.

As described above, PGD_2 is rapidly degraded into several products in blood (10, 11). These products possibly accumulate locally and preferentially stimulate CRTH2-mediated proinflammatory signaling according to disease progression. Indeed, treatment with the major PGD_2 metabolites DK-PGD_2 and 9α,11β-PGF_2 (10 ng per ear) significantly enhanced vascular leakage (Fig. 5F).

The effect of PGD_2 on vascular permeability and neutrophil migration in vitro

We examined the effect of PGD_2 on vascular endothelial permeability by measuring TER in vitro. In line with the in vivo data showing DP-mediated vascular barrier enhancement (Fig. 4E), treatment with PGD_2 (10 μM) or BW 245C (1 μM) elevated TER, indicating barrier enhancement (typical responses are shown in Fig. 6A and summarized in Fig. 6B). These effects were completely inhibited by DP antagonism (BW A868C, 10 μM, 30 min before PGD_2 administration). A CRTH2 agonist, DK-PGD_2 (1 μM), which enhanced vascular permeability in vivo, did not change TER in vitro. In addition, 9α,11β-PGF_2 (1 μM) did not affect endothelial barrier formation in vitro (Fig. 6B).

In the transmembrane migration assay, isolated neutrophils migrated toward a solution of 5 nM leukotriene B_4 added into the lower chamber (Fig. 6C), as previously reported (31). Stimulation with PGD_2 or a DK-PGD_2 (1 μM), 9α,11β-PGF_2 (100 nM), also induced neutrophil migration; this was abolished by CRTH2 antagonism (CAY10471, 1 μM).

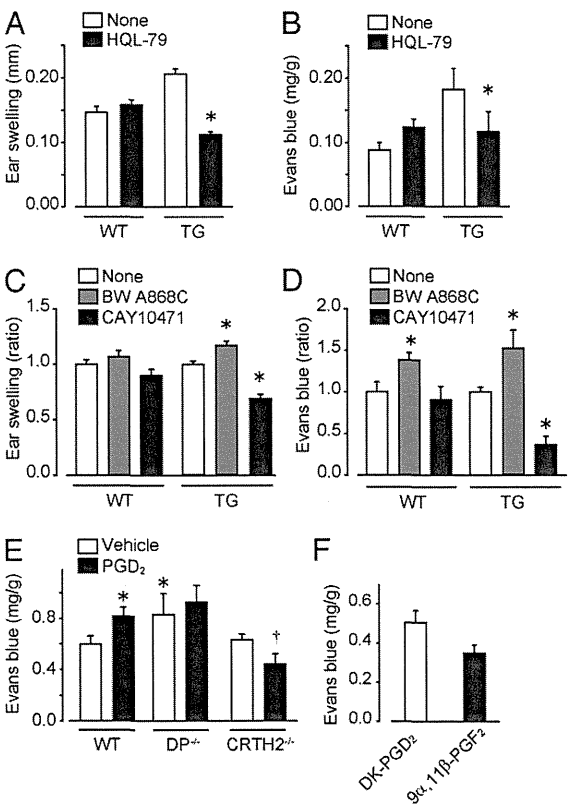

FIGURE 5. CRTH2 signaling promotes late-phase inflammation. Effects of HQL-79 [50 mg/kg, i.p., 3 h before the oil treatment (**A**)] or a DP antagonist, BW A868C [1 mg/kg, i.p., 2 h before the oil treatment (**B**)], or a CRTH2 antagonist, CAY10471 [1 mg/kg, i.p., 30 min before the oil treatment (B) on the late-phase ear swelling (A and **C**) and dye extravasation (B and **D**)]. Dye extravasation during late-phase inflammation was assessed in DP$^{-/-}$ or CRTH2$^{-/-}$ mice with C57BL/6 background (**E**). PGD_2 (1 mg/kg, i.p.) was administered 10 min before the stimulation. Effect of a CRTH2 agonist, DK-PGD_2 (10 ng per ear), or a PGD_2 metabolite, 9α,11β-PGF_2 (10 ng per ear), on vascular permeability in vivo (**F**) (n = 4–9 each, $^*p < 0.05$ compared with nontreated WT ears or CRTH2$^{-/-}$ ears).

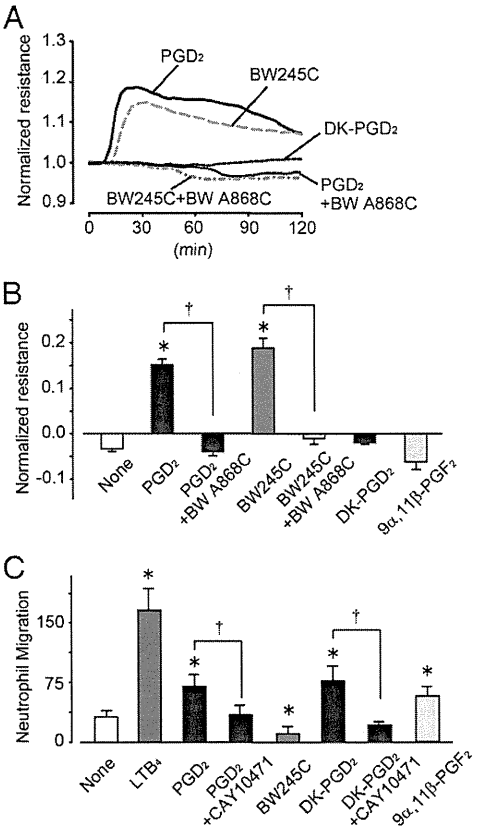

FIGURE 6. The effect of PGD_2 on vascular endothelial barrier formation and neutrophil migration. A representative figure (**A**) or quantification (**B**) of the TER is shown (n = 4–6 each, $^*p < 0.05$ and $^\dagger p < 0.05$ compared with nontreated or stimulant-treated cells). BAECs were treated with PGD_2 (10 μM), BW 245C (1 μM), DK-PGD_2 (1 μM), or 9α,11β-PGF_2 (1 μM). BW A868C (10 μM) was given 30 min before the PGD_2 or BW 245C treatment. Migration assay was performed using isolated neutrophils (**C**). Stimulants were added to the lower chamber, and CAY10471 (1 μM) was added to both the lower and the upper chambers. Data are shown as the number of cells migrating to the lower chamber in one field (×20, n = 5 each, $^*p < 0.05$ and $^\dagger p < 0.05$ compared with nontreated or stimulant-treated cells).

Discussion

Using genetically modified mice that overexpress H-PGDS, we demonstrated that PGD_2 assumes both pro- and anti-inflammatory roles according to the progression of inflammation. Specifically, upon initiation of croton oil–induced dermatitis, PGD_2 produced from tissue resident cells exhibits an anti-inflammatory action through DP-mediated signaling. At the progression phase, PGD_2, and possibly its degradation products secreted from infiltrating leukocytes, promote inflammation through CRTH2-mediated signaling (Supplemental Fig. 4).

At the early phase of dermatitis, secreted PGD_2 had anti-inflammatory activity in both WT and TG mice, which is attributable to DP-mediated signaling. TG showed relatively strong anti-inflammatory reactions. These phenomena are presumably due to the higher level of PGD_2 production in TG ears. The experiments using BMT revealed that PGD_2 produced from tissue resident cells contributes to the anti-inflammatory reaction during the early phase. Given that vascular endothelial cells constitutively express COX-2 (which is indispensable for PGD_2 production), endothelial cell–derived PGD_2 is likely to control inflammation in early-phase dermatitis.

We observed that DP-mediated signaling contributes to the anti-inflammatory role of PGD_2 by enhancing endothelial barrier formation. We previously reported that vascular endothelial cells express DP and its agonism inhibits vascular leakage in the inflamed lung (22) and growing tumor (23), in agreement with our current observations. The underlying molecular mechanism associated with stimulation of DP is tightening of endothelial cell-to-cell junctions through the cAMP/protein kinase A/Rac signaling pathway (32).

Of interest, in contrast to its anti-inflammatory role in the early phase, secreted PGD_2 showed proinflammatory effects in the late phase. When compared with the ears of WT animals, the ears of TG mice had more severe inflammation with increased PGD_2 production. BMT and morphological studies suggested that infiltrating leukocytes produced PGD_2 and promoted tissue swelling and vascular hyperpermeability. Considering the fact that tissue contents of PGD_2 were similar in the early and late phases in each line of mice (Fig. 1D), the site of production seems to be more crucial than the amount of PGD_2 for PGD_2-mediated immune responses.

We further demonstrated that CRTH2 signaling mediates the proinflammatory effects of PGD_2. This activity is likely because many of the PGD_2 degradation products potentially bind CRTH2 (12). Further investigation is required to assess the contribution of each product to the pathogenesis of inflammation, especially in vivo. However, it is possible that sustained local inflammation leads to the accumulation of PGD_2 metabolites, which further accelerate inflammation by acting as CRTH2 ligands.

Our data show that both a CRTH2 agonist ($DK\text{-}PGD_2$) and a major PGD_2 metabolite ($9\alpha,11\beta\text{-}PGF_2$) enhanced vascular permeability in vivo, but they did not directly influence endothelial barrier formation in vitro. Previous studies showed that CRTH2 stimulation promotes the migration of BM-derived hematopoietic lineage cells such as Th2 lymphocytes and eosinophils (33). Consistently, CRTH2 agonism stimulated migration of neutrophils in vitro. In addition, infiltration of neutrophils was accelerated in inflamed TG ears. Neutrophils produce a variety of bioactive agents, including cytokines and reactive oxygen, that can stimulate the vascular bed (34). Thus, neutrophil-derived PGD_2 may promote neutrophil infiltration/migration through CRTH2 signaling, and as a result, bioactive substances released from infiltrating neutrophils could promote inflammation, at least partially, by disrupting the vascular barrier.

Our data showing that the PGD_2–DP signaling axis mediates anti-inflammatory reactions imply that DP agonism may be a strategy for treatment of various inflammatory diseases. Conversely, we also showed in this article that activation of the PGD_2–CRTH2 signal axis in inflammatory cells promotes inflammation. These situations presumably occur in diseases that are accompanied by local accumulation of PGD_2-secreting immune cells, such as allergic inflammation with mast cell and/or eosinophil accumulation. H-PGDS inhibition or CRTH2 antagonism might be beneficial for these pathological conditions.

Inflammation is an indispensable response for the rejection of foreign substances and for tissue regeneration, and it occurs throughout the body. As key players in this response, PGs are likely produced and received by almost all types of cells. To understand and manage various types of inflammatory diseases, a detailed evaluation of the role of individual PG types with respect to their source and effects in each phase of disease is an absolute requirement. We suggest that our use of the H-PGDS TG mice that overexpress H-PGDS with a β-actin promoter provides significant insight in this regard. The system is not without caveats, however, because the inflammatory symptoms observed in the TG mice were induced owing to exogenous expression of H-PGDS driven by a nonnative promoter. However, this mouse model highlighted the role of PGD_2 in inflammation and allowed us to provide deep insights into the paradoxical action of PGD_2.

In summary, the Janus-like behavior of PGD_2 with regard to its pro- and anti-inflammatory effects in vivo was determined by an exquisite balance of multiple factors, which included the site of its production and the quantity of PGD_2 and related degradation products.

Disclosures

The authors have no financial conflicts of interest.

References

1. Stock, J. L., K. Shinjo, J. Burkhardt, M. Roach, K. Taniguchi, T. Ishikawa, H. S. Kim, P. J. Flannery, T. M. Coffman, J. D. McNeish, and L. P. Audoly. 2001. The prostaglandin E2 EP1 receptor mediates pain perception and regulates blood pressure. *J. Clin. Invest.* 107: 325–331.
2. Ushikubi, F., E. Segi, Y. Sugimoto, T. Murata, T. Matsuoka, T. Kobayashi, H. Hizaki, K. Tuboi, M. Katsuyama, A. Ichikawa, et al. 1998. Impaired febrile response in mice lacking the prostaglandin E receptor subtype EP3. *Nature* 395: 281–284.
3. Furci, L., D. J. Fitzgerald, and G. A. Fitzgerald. 1991. Heterogeneity of prostaglandin H2/thromboxane A2 receptors: distinct subtypes mediate vascular smooth muscle contraction and platelet aggregation. *J. Pharmacol. Exp. Ther.* 258: 74–81.
4. Bingham, C. O., III 2002. Development and clinical application of COX-2-selective inhibitors for the treatment of osteoarthritis and rheumatoid arthritis. *Cleve. Clin. J. Med.* 69(Suppl 1): SI5–SI12.
5. Gupta, R. A., and R. N. Dubois. 2001. Colorectal cancer prevention and treatment by inhibition of cyclooxygenase-2. *Nat. Rev. Cancer* 1: 11–21.
6. Qu, W. M., Z. L. Huang, X. H. Xu, K. Aritake, N. Eguchi, F. Nambu, S. Narumiya, Y. Urade, and O. Hayaishi. 2006. Lipocalin-type prostaglandin D synthase produces prostaglandin D2 involved in regulation of physiological sleep. *Proc. Natl. Acad. Sci. USA* 103: 17949–17954.
7. Eguchi, N., T. Minami, N. Shirafuji, Y. Kanaoka, T. Tanaka, A. Nagata, N. Yoshida, Y. Urade, S. Ito, and O. Hayaishi. 1999. Lack of tactile pain (allodynia) in lipocalin-type prostaglandin D synthase-deficient mice. *Proc. Natl. Acad. Sci. USA* 96: 726–730.
8. Kostenis, E., and T. Ulven. 2006. Emerging roles of DP and CRTH2 in allergic inflammation. *Trends Mol. Med.* 12: 148–158.
9. Suzuki, F., H. Hayashi, and O. Hayaishi. 1986. Transport of prostaglandin D2 into brain. *Brain Res.* 385: 321–328.
10. Fitzpatrick, F. A., and M. A. Wynalda. 1983. Albumin-catalyzed metabolism of prostaglandin D2. Identification of products formed in vitro. *J. Biol. Chem.* 258: 11713–11718.
11. Kikawa, Y., S. Narumiya, M. Fukushima, H. Wakatsuka, and O. Hayaishi. 1984. 9-Deoxy-delta 9, delta 12-13,14-dihydroprostaglandin D2, a metabolite of prostaglandin D2 formed in human plasma. *Proc. Natl. Acad. Sci. USA* 81: 1317–1321.
12. Sawyer, N., E. Cauchon, A. Chateauneuf, R. P. Cruz, D. W. Nicholson, K. M. Metters, G. P. O'Neill, and F. G. Gervais. 2002. Molecular pharmacology of the human prostaglandin D2 receptor, CRTH2. *Br. J. Pharmacol.* 137: 1163–1172.